NO-stressed *Y. pseudotuberculosis* have decreased cell division rates in the mouse spleen

Running title: Fluorescence dilution detects slowed bacterial growth

Bessie Liu[1], Robert K. Davidson[1], Kimberly M. Davis[1,*]

[1]W. Harry Feinstone Department of Molecular Microbiology and Immunology
Johns Hopkins Bloomberg School of Public Health, Baltimore, MD, USA

*Corresponding author:
E-mail: kdavi140@jhu.edu

Abstract

Fluorescence dilution approaches can detect bacterial cell division events, and can detect if there are differential rates of cell division across individual cells within a population. This approach typically involves inducing expression of a fluorescent protein, and then tracking partitioning of fluorescence into daughter cells. However, fluorescence can be diluted very quickly within a rapidly replicating population, such as pathogenic bacterial populations replicating within host tissues. To overcome this limitation, we have generated a revTetR reporter construct, where mCherry is constitutively expressed, and repressed by addition of tetracyclines, resulting in fluorescence dilution within defined timeframes. We show that mCherry signal is diluted in replicating populations, and that mCherry signal accumulates in growth-inhibited populations, including during exposure to inhibitory concentrations of antibiotics and during nitric oxide exposure. Furthermore, we show that tetracyclines can be delivered to the mouse spleen during *Yersinia pseudotuberculosis* infection. We defined a drug concentration that results in even exposure of cells to tetracyclines, and used this system to visualize cell division within defined timeframes post-inoculation. revTetR mCherry signal did not appear enriched in a particular spatial location within replicating centers of bacteria. However, the addition of a NO-sensing reporter (P_{hmp}*::gfp*) showed that heightened NO exposure correlated with heightened mCherry signal, suggesting decreased cell division within this subpopulation. This revTetR reporter will provide a critical tool for future studies to identify and isolate slowly replicating bacterial subpopulations from host tissues.

Introduction

Bacterial growth and metabolism have been the focus of decades of research, in part because we need to learn more about the pathways utilized by bacteria for growth to be able to target these essential processes with antibiotics or novel therapeutics. It is also well appreciated that bacteria with slowed metabolic rates are less susceptible to antibiotics (1-4). Earlier studies focused on growth of bacteria and antibiotic susceptibility under different laboratory conditions (1, 5-7); more recently, there has been a focus on studying bacterial growth and metabolism within host tissues, to more closely approximate bacterial growth conditions at the point where antibiotics or other therapeutics would be administered (8-10). Importantly, bacterial pathogens may utilize a range of different nutrients for growth within host tissues, and individual bacteria, or subsets of bacteria, may concurrently utilize different metabolites to promote their growth (10-14). Some of these substrates may support faster bacterial replication rates, and others, slower replication rates. Nutrient availability and the presence of host-derived antimicrobials, in addition to interactions with different immune cells subsets, can also generate complex microenvironments within host tissues, which can result in differences in growth rates across bacterial populations (12, 15-18).

When treating a bacterial infection, differences in bacterial growth rates can dramatically impact antibiotic efficacy. Slow-growing subsets of bacteria are inherently less susceptible to antibiotic treatment, due to decreased metabolic rates (1, 3, 4). This is termed antibiotic tolerance, a transient, phenotypic change in a subset of bacterial cells within a population, which alters antibiotic susceptibility (19, 20). Many of these experiments have been performed in bacteriological media, so it still remains largely unclear which pathways promote decreased antibiotic susceptibility and slowed growth within host tissues. To identify these pathways,

62 investigators will need to isolate antibiotic tolerant cells from the host environment for
63 downstream analyses. The specific bacterial pathways linked to tolerance may depend in part on
64 the antibiotic and the mode of action, or the environment around the bacteria during the
65 antibiotic exposure (18, 21, 22).

66 Molecular tools currently exist to identify and isolate slow-growing bacterial cells (8, 23-
67 26), but there are also limitations with some of these approaches that need to be addressed to
68 apply them within the host environment. One of the main approaches is utilizing fluorescence
69 dilution to identify individual cells that have divided within a certain timeframe. Typically,
70 fluorescence dilution approaches involve inducing expression of a fluorescent protein then
71 removing the inducer, and detecting changes in the amount of fluorescent protein within cells as
72 a readout for cell division events and protein partitioning into daughter cells (27, 28). Many
73 research groups have successfully utilized this approach to identify dividing and non-dividing
74 bacterial cells, by inducing fluorescent expression prior to introducing bacteria into tissue culture
75 or infection models (27-30). For some bacterial infection models, this approach can easily be
76 applied, because the size of the colonizing population of bacteria is relatively large, and the
77 number of cell division events within host tissues is relatively small (24, 25, 27). However, in
78 other infection models, only a few bacterial cells establish infection, and these cells go on to
79 replicate many times, which would quickly dilute out fluorescent signals (17, 31-33).
80 Furthermore, it is difficult to deliver inducer compounds into host tissues at sufficient levels to
81 modulate gene expression, and more challenging to remove these compounds to allow for
82 subsequent fluorescence dilution.

83 *Yersinia pseudotuberculosis* is an enteric pathogen that spreads systemically from
84 intestinal tissues to colonize deep tissue sites, such as the spleen (34-36). There is a strong

85 population bottleneck within intestinal tissues, and few bacterial cells spread systemically to
86 colonize deep tissue sites (37). Within deep tissues, individual bacteria found clonal clusters of
87 replicating extracellular bacteria, termed microcolonies or pyogranulomas (17, 38, 39).
88 Microcolonies can grow to contain hundreds to thousands of bacteria within a single replication
89 site, despite recruitment of circumscribing layers of neutrophils and monocytes (17, 39, 40).
90 Recent studies have shown that subpopulations of bacteria are present within microcolony
91 structures, and that subsets of bacteria stressed by the presence of nitric oxide (NO)
92 preferentially survive treatment with doxycycline, suggesting they may represent a slow-growing
93 subset of cells (17, 22). However, it has been difficult to determine growth rates in this model
94 system, since fluorescence dilution approaches cannot typically be used when the bacterial
95 population contracts and expands so dramatically.

96 To overcome these limitations, we have generated a revTetR reporter construct, where
97 exposure to tetracyclines will inhibit additional fluorescent gene expression, resulting in
98 fluorescence dilution. This construct will promote fluorescent signal accumulation in non-
99 dividing cells, and fluorescent protein will be diluted into dividing cells, thus allowing us to
100 differentiate between dividing and non-dividing subpopulations of bacteria. Tetracyclines can
101 also easily be delivered into our mouse model of *Yersinia pseudotuberculosis* systemic infection
102 (22), which allows us to visualize fluorescence dilution as a measure of cell division at specific
103 stages of infection and within specific timeframes. Here, revTetR allows us to ask if responses to
104 host-derived stresses, specifically nitric oxide (NO), impacts *in vivo* cell division rates. This
105 reporter construct will be a useful tool for future studies to isolate and characterize bacterial
106 subpopulations with differential growth rates.

107 **Results**

108 **The revTetR reporter can be used to visualize differential bacterial growth rates *in vitro***
109 **with mCherry fluorescence dilution.**

110 To detect differential cell division rates within host tissues, we generated a fluorescence
111 dilution reporter system by modifying our recently described TetON fluorescent reporter with
112 stable mCherry (*tetR*::P_{tetA}*::mCherry*) (22). The revTetR reporter (*revtetR::*P_{tetA}*::mCherry*) was
113 constructed by introducing two mutations (E15A and L17G) into the wild-type *tetR* gene. These
114 two mutations were predicted to cause a reversal of TetR activity resulting in repression of P_{tetA}
115 specifically in the presence of tetracycline and tetracycline derivatives (41, 42). Therefore,
116 revTetR is a tetracycline-responsive reporter that allows cells to constitutively express mCherry
117 in the absence of tetracycline derivatives, and subsequent addition of tetracyclines should inhibit
118 additional mCherry transcription **(Figure 1A)**. This reporter can be used to compare growth rates
119 of bacteria via a fluorescence dilution approach (27, 28). For example, in cultures treated with
120 tetracycline, fast-growing cells will continue to divide, and the existing mCherry signal will be
121 partitioned between daughter cells with every replication event **(Figure 1B)**. However, slow-
122 growing or nondividing cells will not go through the same number of replication events and
123 therefore will not undergo fluorescence dilution **(Figure 1B)**.

124 To confirm that the mCherry fluorescence from the revTetR reporter dilutes into actively
125 dividing cells, we generated a reporter strain containing the revTetR reporter alongside a plasmid
126 containing *dps::gfp-ssrA* (revTetR *dps*) (16). Dps, a ferritin-like iron-sequestering protein,
127 accumulates within bacteria in stationary phase in response to multiple different stresses and
128 protects DNA from oxidative damage (43-45). Therefore, revTetR *dps* should detect slow-
129 growing cells within the population with GFP signal (16), and allow us to compare this to

130 mCherry levels from revTetR. Exponential phase revTetR *dps* cells were treated with increasing
131 doses of anhydrotetracycline (ATc), a tetracycline derivative that binds TetR or revTetR but has
132 limited ribosomal targeting (46, 47). Aliquots of each sample were measured for optical density
133 or absorbance (A_{600nm}) and fluorescence using a microplate reader. The absorbance values
134 increased across all treatment groups, and ATc did not have a detrimental effect upon growth
135 rate with either 0.1µg/ml or 1µg/ml treatment **(Figure 1C)**. However, 2µg/ml ATc treatment did
136 slightly inhibit growth, resulting in significantly lower OD values at 3h and 4h post-treatment
137 (hours, h). mCherry fluorescence values were normalized to cell number by dividing the
138 background-subtracted fluorescence value from each well by the corresponding OD value. The
139 resulting value was further normalized to the untreated sample value for each time point (set at
140 100%). Following 2h of ATc treatment, all treated groups had significantly reduced mCherry
141 fluorescence relative to untreated cells **(Figure 1D).** This was consistent with a predicted 1.5-2h
142 cell division rate during growth at 37ºC based on absorbance **(Figure 1C)**. At 4h post-treatment,
143 the fluorescence signal for all treated groups decreased by approximately 40% relative to the
144 signal of the untreated group, showing that ATc successfully induces dilution of mCherry with
145 each replication event **(Figure 1D)**. We noted that 2µg/ml ATc treatment resulted in
146 significantly higher mCherry **(Figure 1D)** and *dps* reporter signal **(Figure 1E)** relative to
147 0.1µg/ml and 1µg/ml treatment, again suggesting the dose may slightly inhibit growth, and
148 providing evidence that slowed growth can be detected by an increase in mCherry signal.
149 Heterogeneity within each sample was further represented at the single-cell level. Cells
150 from the final time point (4h) were fixed and imaged using fluorescence microscopy, and
151 analyzed for single cell fluorescence measurements. The average signal of the untreated group
152 (0µg/ml) was significantly higher than the average signal of the group treated with the lowest

153 dose of ATc (0.1µg/ml), again showing that signal dilution was successful **(Figure 1F)**. 1µg/ml
154 ATc treated cells had mCherry fluorescence similar to the 0.1µg/ml treated group. However, at
155 the highest dose of ATc (2µg/ml), the average mCherry signal signficantly increased **(Figure**
156 **1F)**, and we found there were also significant increases in *dps* reporter expression with
157 increasing doses of ATc **(Figure 1G)**, suggesting that high concentrations of ATc may have an
158 inhibitory effect on bacterial cells. Slower growing cells with heightened *dps* reporter expression
159 should also exhibit heightened revTetR mCherry signal, and we confirmed these signals were
160 correlated under all treatment conditions, based on significantly non-zero slopes of linear
161 regression best-fit lines **(Figure 1H)**. Collectively these data indicate that revTetR fluorescence
162 is accumulating in slow-growing cells, and that actively growing cells are partitioning mCherry
163 into daughter cells, resulting in significant decreases in mCherry signal.
164
165 **Growth inhibition with doxycycline promotes mCherry fluorescence accumulation.**
166 To further test whether growth-inhibited cells exhibit heightened revTetR mCherry
167 fluorescence, cells of the revTetR *dps* strain were sub-cultured to exponential phase and treated
168 with increasing doses of the antibiotic, doxycycline (Dox). Aliquots of each sample were
169 measured for optical density (OD) by absorbance (A_{600nm}) and fluorescence at hourly timepoints
170 using a microplate reader. Cells exposed to 1µg/mL Dox had significantly decreased growth rate,
171 however the doses less than 1µg/ml (0.01-0.1µg/ml) were subinhibitory, and did not impact
172 growth **(Figure 2A)**. mCherry fluorescence was initially heightened with 1µg/ml Dox treatment
173 **(Figure 2B)**, and *dps* reporter signal was slightly, but not significantly, elevated **(Figure 2C)**,
174 consistent with growth inhibition at this treatment concentration. Three hours after treatment, the
175 mCherry signal in all treatment groups was significantly below untreated values, including the

176 1µg/ml treatment group **(Figure 2B)**, suggesting that growth may resume after initial growth
177 inhibition. Single cell analysis was performed by fluorescence microscopy, and single cell
178 fluorescence levels were graphed for each treatment group. Dilution of mCherry signal could be
179 seen with treatment of 0.01µg/mL Dox, but as the dosage increased, the mean mCherry signal
180 within cells increased, indicating signal accumulation and stalled growth **(Figure 2D)**. The
181 mCherry fluorescent signal was significantly higher in cells treated with 1µg/ml Dox compared
182 to untreated cells (0µg/ml), suggesting that growth inhibition resulted in significant mCherry
183 revTetR fluorescence accumulation. Again, we observed a correlation between *dps* reporter
184 signal and revTetR mCherry signal under all treatment conditions, confirming that slower
185 growing cells have heightened revTetR fluorescence **(Figure 2E)**.
186
187 **Gentamicin treatment confirms mCherry fluorescence levels are heightened in growth**
188 **arrested cells.**
189 Although subinhibitory treatments with tetracyclines result in fluorescence dilution in
190 actively dividing cells, we observed quite a bit of heterogeneity in revTetR mCherry
191 fluorescence at the single cell level. To address the high variability of data from the previous
192 fluorescence dilution experiments, we used a short gentamicin treatment to inhibit growth and
193 synchronize the cell cycle of sampled populations before removing the antibiotic to allow growth
194 to resume. Gentamicin was chosen for these experiments because it is an aminoglycoside that
195 targets the ribosome to inhibit bacterial growth, but does not interact with revTetR. We initially
196 tested three concentrations of gentamicin to identify a concentration that might synchronize the
197 bacterial population: 5µg/ml, 10µg/ml, and 40µg/ml; we added gentamicin at 0h, and then
198 monitored growth based on absorbance in the presence of gentamicin. 5µg/ml did not

199 significantly impact growth, while 40µg/ml resulted in growth inhibition, and 10µg/ml had an
200 intermediate effect on growth **(Figure 3A)**. Only the 40µg/ml dose resulted in an increase in
201 mCherry fluorescence, which was apparent after 1h treatment **(Figure 3B)**, and so we chose to
202 perform subsequent experiments with the inhibitory 40µg/ml dose for only an hour incubation,
203 anticipating that cells would resume growth after washing out gentamicin and adding cells to
204 fresh media. revTetR *dps* cells were treated with gentamicin for 1 hour, washed with fresh media
205 to allow their growth to resume, and then treated with ATc (1µg/ml). OD and fluorescence were
206 measured up to 4h post ATc treatment. The sum mCherry fluorescence (total fluorescence per
207 cell) was significantly higher in the gentamicin-treated sample immediately prior to ATc
208 treatment, however there was still high variability in mCherry expression, suggesting gentamicin
209 treatment did not promote uniform mCherry accumulation **(Figure 3C)**. Additionally, cells
210 treated with gentamicin did not resume growth following treatment based on OD measurements
211 **(Figure 3D)**. Consistent with this, mCherry signal was only slightly lower in gentamicin-treated
212 cells treated with ATc, suggesting very little growth 4h following gentamicin treatment **(Figure**
213 **3E)**. Cells that were not treated with gentamicin exhibited normal growth, and significant
214 fluorescence dilution with ATc treatment **(Figure 3E)**. These data suggest that growth arrest
215 does result in significant mCherry signal accumulation, but the addition of gentamicin prior to
216 ATc treatment did not reduce variability in mCherry signal at the single cell level.
217

218 **Nitric oxide-stressed cells divide at a slower rate than unstressed cells.**

219 It has been shown recently that exposure to nitric oxide (NO) results in cell division
220 arrest, through collapse of the FtsZ cell division machinery (48). Our results have also suggested
221 NO-stressed *Yersinia pseudotuberculosis* preferentially survive doxycycline treatment during

222 growth in the mouse spleen (22), which is consistent with a hypothesis that NO causes cell
223 division arrest within host tissues, and subsequently promotes decreased antibiotic susceptibility.
224 Cells containing the revTetR reporter and $P_{hmp::}$*gfp* (revTetR $P_{hmp::}$*gfp*) were treated with
225 the slow-releasing NO donor compound DETA-NONOate for 1h, then further treated with ATc
226 (1µg/ml). The $P_{hmp::}$*gfp* reporter was used to detect NO exposure, and to mark the level of stress
227 experienced by individual cells, which can be variable across the population in response to
228 DETA-NONOate (16, 17). Aliquots were taken every 2h after ATc treatment, and fixed cells
229 were imaged using fluorescence microscopy at the indicated timepoints (**Figure 4A**). Images
230 were subsequently quantified for single-cell fluorescence measurements. Growth inhibition due
231 to treatment with the NO donor, DETA-NONOate, was confirmed **(Figure 4B)**; induction of
232 *hmp* above the baseline level in response to the NO donor was also confirmed across all
233 treatment groups **(Supplemental Figure 1)**. When comparing cells treated with NO and ATc, we
234 found the revTetR mCherry fluorescence remained high and actually increased between 2h and
235 4h ATc treatment, consistent with growth inhibition in the presence of NO **(Figure 4C)**. In
236 contrast, cells grown in the absence of NO treatment had a significant drop in mCherry
237 fluorescence between 2h and 4h, suggesting significant levels of cell division events within this
238 timeframe **(Figure 4C)**. Consistent with previous literature, these results indicate that NO
239 treatment results in growth arrest, and reduced levels of cell division events (48).
240 To determine if cell division occurred in cultures despite NO stress, and whether
241 heightened *hmp* reporter signal correlated with heightened revTetR mCherry signal, single cell
242 mCherry and GFP levels from NO-treated cells were compared in the presence and absence of
243 ATc treatment using correlation plots. At the time of ATc treatment (0h) the bacterial
244 populations were very similar in fluorescence, as expected **(Figure 4D)**. At 2h post-ATc

245 addition, there was a correlation between mCherry and GFP levels independent of ATc
246 treatment, and extensive overlap within the cell populations, suggesting few cell division events
247 within this timeframe **(Figure 4D)**. However, at 4h post-ATc treatment, there was a clear
248 decrease in mCherry fluorescence, suggesting cell division had occurred despite NO treatment,
249 and there was a positive correlation between mCherry and GFP levels in NO-stressed cells
250 treated with ATc, which was lost in -ATc samples **(Figure 4D)**. These data suggest that while
251 NO-treated cells can continue to replicate after treatment, cells experiencing higher levels of
252 stress, as evidenced by higher *hmp* reporter signal, completed fewer cell division events over the
253 timecourse than cells experiencing lower levels of stress.
254

255 **Low doses of doxycycline and anhydrotetracycline diffuse evenly across microcolonies and**
256 **do not inhibit bacterial growth.**

257 One of the major goals for generating the revTetR reporter was to set-up a system to
258 detect bacterial cell division events within host tissues over defined periods of time. To do this,
259 we would need to administer tetracyclines during infection, and ensure that the dosage used
260 would not impact bacterial growth, and also diffuse evenly across microcolonies to allow for
261 accurate detection of signal dilution and cell division. We have previously developed a model of
262 doxycycline treatment of *Y. pseudotuberculosis* infection, and found that a single 40mg/kg
263 injection of doxycycline significantly reduces bacterial CFUs and also accumulates at a higher
264 concentration at the periphery of microcolonies (22). We hypothesized that lowering the
265 tetracycline dose may allow us to administer sub-inhibitory levels of antibiotic that would still
266 modulate the revTetR reporter, while allowing for more even diffusion of the antibiotic across
267 microcolonies.

268 To identify a tetracycline concentration that results in equal diffusion across
269 microcolonies, a previously characterized reporter, P_{tetA}*::mCherry-ssrA* (TetON), was used for
270 tetracycline detection (22). The TetON reporter contains the wild-type *tetR* gene; addition of
271 tetracyclines induce the production of mCherry, and therefore levels of mCherry can be used as a
272 readout for antibiotic exposure **(Figure 5A)**. C57BL/6 mice were inoculated intravenously with
273 the TetON gfp^+ strain, which has constitutive expression of GFP alongside the TetON reporter,
274 allowing for visualization of relative reporter expression. A single dose of 4mg/kg Dox or
275 4mg/kg ATc was administered intraperitoneally at 48 hours post-inoculation. This timepoint was
276 chosen for antibiotic administration since we can detect subsets of bacteria responding to host-
277 derived nitric oxide at this timepoint, thus allowing us to ask whether stressed subpopulations of
278 bacteria are dividing more slowly than unstressed bacteria.
279 At 4h or 24h post-treatment, spleens were harvested to quantify CFUs and quantify
280 reporter expression by fluorescence microscopy. Bacterial numbers continued to increase
281 between 4h and 24h post-treatment with 4mg/kg doses of either ATc or Dox, confirming this
282 dosage does not interfere with bacterial growth **(Figure 5B)**. Microcolonies were then visualized
283 by fluorescence microscopy to determine if ATc and Dox diffuse evenly across microcolonies at
284 this dosage. The centroid and periphery of each microcolony were quantified for mCherry and
285 GFP signal, and the ratio of mCherry/GFP was graphed. There were no significant differences in
286 mCherry/GFP ratios between the centroid and periphery of microcolonies treated with either
287 ATc or Dox, suggesting that each drug was diffusing evenly across microcolonies **(Figure 5C)**.
288 The mCherry/GFP ratios remained comparable at the centroid and peripheries even at 24 hours
289 after treatment, showing that throughout the infection time course, there was even diffusion of
290 the drugs **(Figure 5C, 5D)**. These data here suggest that lowering the tetracycline dosage 10-fold

291 results in even diffusion of a sub-inhibitory dose of tetracyclines, which will allow us to
292 modulate revTetR reporter expression in all cells across the microcolony without impacting
293 bacterial growth.
294
295 **revTetR signal appears to increase in both the centroid and periphery of microcolonies.**
296 To determine if there are slowly-dividing subpopulations of bacteria within
297 microcolonies, we infected mice with the revTetR *gfp*$^{+}$ strain, and treated mice with ATc at 48h
298 post-inoculation or left mice untreated. Mice were sacrificed at either 4h or 24h post-treatment,
299 and spleens were harvested to quantify CFUs and visualize reporter expression by fluorescence
300 microscopy. Bacterial CFUs were comparable between ATc-treated and untreated mice at both
301 timepoints, suggesting that ATc treatment did not impair bacterial growth **(Figure 6A)**.
302 However, we did not see an increase in CFUs between 4h and 24h, which suggests there was
303 limited, or variable, bacterial growth within this selected timeframe for this bacterial strain. To
304 determine if there were differences in reporter expression, mCherry signal was quantified
305 relative to the constitutive GFP signal at the periphery and centroid of individual microcolonies.
306 Since we have previously shown that bacteria experience heightened levels of NO stress and
307 express higher levels of the T3SS at the periphery of microcolonies, we were expecting to see
308 heightened levels of mCherry signal relative to GFP at the periphery of microcolonies. At 4h
309 post-treatment, we did not observe any differences in mCherry signal at the periphery of
310 microcolonies compared to the centroid, in the absence or presence of ATc treatment **(Figure
311 6B)**. This suggested there may not have been many cell division events within the first 4h of
312 treatment, which is why tissue was also harvested 24h post-treatment. At 24h post-treatment,
313 untreated mice had significantly lower levels of mCherry signal at the periphery of

314 microcolonies, and ATc treated mice also had significantly lower mCherry signal at the
315 periphery, indicating we were not seeing increased mCherry signal at the periphery of
316 microcolonies as expected **(Figure 6C)**. It did appear that ATc treated microcolonies had higher
317 mCherry signals at both the centroid and periphery relative to untreated microcolonies, although
318 this was not statistically significant. These results suggest that revTetR signal remained high
319 after ATc treatment, indicating there may be slowly dividing cells present within microcolonies,
320 but it was difficult to assess whether these cells were part of a particular subpopulation of
321 bacteria without an additional reporter alongside revTetR.
322
323 **NO stress correlates with heightened mCherry signal accumulation and slowed cell division**
324 **rates.**
325 Hmp$^+$ bacteria responding to NO stress preferentially survive doxycycline treatment,
326 suggesting they may represent a slow-growing subpopulation (22). Consistent with this, in
327 culture NO stressed cells accumulated heightened mCherry signal, suggesting they were dividing
328 more slowly than unstressed cells **(Figure 4)**. However, in our mouse model it was difficult to
329 determine if peripheral cells of the microcolony had heightened revTetR signal without marking
330 the peripheral subpopulation with the *hmp* reporter. To determine if NO-stressed bacteria are
331 dividing more slowly than unstressed cells within host tissues, we infected mice with the
332 revTetR P_{hmp}*::gfp* strain and treated mice with ATc at 48h post-inoculation, or left mice
333 untreated. Spleens were harvested at 4h and 24h post-treatment to quantify CFUs and visualize
334 reporter expression by fluorescence microscopy. CFUs within ATc-treated mice did not differ
335 significantly from CFUs within untreated mice; again, we noted that there was not significant
336 growth based on total CFUs between 4h and 24h, but anticipated that there would be sufficient

337 replication at the level of individual microcolonies to assess differences in revTetR signal
338 **(Figure 7A)**.
339 Periphery and centroid measurements were taken from each microcolony image and
340 combined into a single periphery/centroid ratio for each microcolony to allow for comparison
341 across treatment groups. At 4h post-treatment, the average ratio for the *hmp* reporter signal was
342 above a value of 1, indicating higher expression in the peripheral cells, while the average ratio
343 for mCherry values was close to 1, suggesting equal expression in peripheral and centroid cells
344 **(Figure 7B)**. At 24h post-treatment, GFP ratios remained above 1, indicating high peripheral
345 expression, and the +ATc mCherry ratio appeared to increase, although this was not significant
346 **(Figure 7C)**. There were no significant differences between ATc-treated and untreated groups
347 for either timepoint, suggesting there wasn't a dramatic change in fluorescent signals following
348 ATc treatment in these experiments. However, the slight increase in mCherry expression at 24h
349 indicates that microcolonies may have higher mCherry signal along the periphery, indicating
350 slower growth in that region. Moreover, after the data was separated according to spatial location
351 within the microcolony, there was a clear difference in trends between centroid bacteria and
352 peripheral bacteria **(Figure 7D-G)**. Of note, centroid bacteria showed very similar fluorescent
353 patterns at 4h **(Figure 7D)** and 24h **(Figure 7F)** post-treatment, while peripheral bacteria at 24h
354 post-treatment have a statistically significant positive correlation **(Figure 7G)**, indicating that
355 Hmp^+ cells expressing higher levels of GFP tended to also express higher levels of mCherry
356 **(Figure 7H)**, supporting the conclusion that these cells are slower growing.

357 **Discussion**

358 In this study, we have developed a revTetR mCherry construct that can be utilized to
359 detect bacterial cell division events within host tissues using a fluorescence dilution approach.
360 We have shown this construct results in heightened mCherry signal in growth-arrested cells in
361 culture, and have also shown that nitric oxide (NO) stress is sufficient to promote increased
362 mCherry signal **(Figure 4)**. This was consistent with previous studies showing NO exposure
363 results in an arrest of cell division (48). However, our *in vivo* results in the mouse model of
364 infection were less clear; with a constitutive *gfp* alongside the revTetR reporter, it was difficult to
365 detect the expected heightened mCherry fluorescent signal within peripheral cells **(Figure 6)**,
366 which should have been responding to NO stress. Using the *hmp* reporter alongside revTetR, we
367 were able to show that there was in fact a correlation between *hmp* reporter signal and revTetR
368 mCherry signal within host tissues, suggesting that there were fewer cell division events within
369 the peripheral Hmp^+ population during the selected timeframe of ATc treatment **(Figure 7)**.

370 There are several reasons this association between cell divisions events and NO stress
371 may have been difficult to capture within host tissues. It is possible that we chose a timeframe
372 where there were limited amounts of cell division. In the future, we would like to sample an
373 extended timecourse with the revTetR P_{hmp}*::gfp* strain to better understand where there are larger
374 expansions in the bacterial population, and where we may detect more differential in terms of
375 cell division rates between stressed and unstressed cells. *hmp* expression levels will also need to
376 be assessed at each timepoint to determine if this stressed subpopulation is present. Although this
377 data has previously been generated with other *Y. pseudotuberculosis* strains (17, 22, 49), the low
378 levels of growth between 4h-24h treatment (52h-72h post-inoculation) with the revTetR strains
379 suggest these reporter strains may not be replicating as quickly, or with the same dynamics, as

380 other strains. We would typically expect a 5-10 fold increase in bacterial growth within this
381 timeframe, as seen with the TetON *gfp*$^{+}$ strain **(Figure 5B)**. Another useful approach may be to
382 modulate revTetR mCherry levels by decreasing initial mCherry expression, which could be
383 interfering with growth of the strain (50). This could be accomplished by integrating a single
384 copy into the chromosome to reduce copy number or by modifying the mCherry start codon to
385 reduce levels of translation initiation (51). One thing to note is that the revTetR reporter strains
386 did grow normally in culture, suggesting if they do have some growth delay, this is specifically
387 induced within the host environment.

388 In this study, we compared revTetR reporter signal during treatment with two tetracycline
389 derivatives, the active antibiotic, doxycycline (Dox), and the inactive derivative,
390 anhydrotetracycline (ATc). Both tetracycline derivatives bind to TetR and revTetR, however
391 ATc is predicted to bind these proteins with higher affinity, and has poor affinity to bacterial
392 ribosomes (46, 47). This allowed us to modulate revTetR with ATc without significantly
393 inhibiting translation, however we would expect to see translational inhibition during Dox
394 treatment, and did see evidence of this when detecting *dps* reporter signal alongside revTetR.
395 The amount of *dps* signal may not significantly increase with Dox treatment due to significant
396 translational inhibition, and the inability of cells to translate *gfp* transcripts, which was observed
397 when growth inhibition with 1µg/ml Dox did not significantly increase GFP signal **(Figure 2C)**.
398 However, we were able to conclude that slow-growing or growth-arrested cells had higher levels
399 of revTetR mCherry signal using ATc and NO treatments.

400 Another consideration for this study was the ability of tetracyclines to diffuse evenly
401 across microcolonies, as high levels of doxycycline were shown to accumulate at the periphery
402 of bacterial microcolonies (22). We were able to identify a tetracycline concentration that

403 resulted in even diffusion across microcolonies **(Figure 5)**, but also pursued a dual reporter
404 strategy to simultaneously detect tetracycline exposure and fluorescence dilution. We chose to
405 generate this construct using a TetON *yfp* construct (*tetR::*P_{tetA}*::yfp*) fused to a mutated
406 P_{tetA}*::mCherry.* Specifically, we mutated the two *tet* operator sites within P_{tetA} at the M3 or M6
407 positions to reverse TetR binding to these sites (52, 53). Although these mutations were
408 predicted to reverse TetR binding, unfortunately we found TetR could no longer bind the M3 or
409 M6 mutated P_{tetA}, which instead resulted in constitutive mCherry expression. As the low
410 concentrations of tetracyclines appeared to diffuse evenly in host tissues, we didn't pursue other
411 routes of generating a dual system.
412 It is also possible that NO stress is such a transient occurrence within host tissues, that
413 this doesn't have prolonged effects on cell division rates, thus making it very difficult to capture
414 growth-arrested cells. This was recently shown with a slow-folding fluorescent protein
415 derivative, $DsRed_{42}$, where NO stress was sufficient to promote fluorescence accumulation, but
416 there was limited overlap in slow-growing and NO-stressed populations within host tissues (16).
417 Destabilized and stable versions of fluorescent proteins were used here to show that NO stress
418 was transient within host tissues, and that few bacteria were actively responding and detoxifying
419 NO at any given timepoint (16). However, the fact that Hmp^+ bacteria preferentially survive
420 doxycycline treatment suggests that, while NO exposure may be transient, there may also be a
421 long-term impact and sustained changes within cells exposed to high levels of NO (22).
422 Although *Yersinia* repairs itself in response to this stress (49), there may be long-term damage,
423 or even genetic changes that occur in response to NO. It would be very interesting to determine
424 if genetic changes occur within microcolonies over the course of infection, especially given these

425 bacterial populations are clonal, founded by single bacterium, and presumed to be genetically

426 homogenous (17).

427 **Materials and Methods**

428 *Bacterial strains and growth conditions.* *Y. pseudotuberculosis* IP2666 was used as the wild-
429 type strain throughout. For *in vitro* experiments, overnight cultures were grown in LB at 26°C
430 with rotation for 16 hours. Exponential phase cultures were sub-cultured at 1:100 into LB, and
431 grown at 37°C with rotation for 2 hours in preparation for experiments. For all mouse infections,
432 bacterial inocula were grown overnight (16 hours) to post-exponential phase in 2xYT broth (LB,
433 with 2x concentration of yeast extract and tryptone) at 26°C with rotation.

434

435 *revTetR reporter construction*. The revTetR reporter was generated by introducing specific point
436 mutations into our previously described *tetR::*P_{tetA}*::mCherry* reporter construct in pMMB67EH
437 (22). *tetR* was mutated by site-directed mutagenesis at two sites, E15A (GAG→GCU) and L17G
438 (CUU→GGU), using 4 point mutations to generate the revTetR construct. An additional L25V
439 mutation could not be successfully introduced. Primers were designed that contained the desired
440 mutations, and were used to PCR amplify around the pMMB67EH plasmid using PfuUltra II
441 high-fidelity polymerase (Agilent). PCR products were purified (QIAGEN) and transformed into
442 electrocompetent DH5αλpir *E. coli.* Colonies were screened based on mCherry fluorescence in
443 the absence of tetracyclines, plasmids were then isolated using the PureYield Plasmid Midiprep
444 kit (Promega), and sequenced to confirm mutations. *revtetR::*P_{tetA}*::mCherry* plasmids were
445 transformed into *Y. pseudotuberculosis* strains as previously described (54), to generate the
446 following reporter strains: *revtetR::*P_{tetA}*::mCherry* P_{dps}*::gfp-ssrA*, *revtetR::*P_{tetA}*::mCherry* gfp^+,
447 and *revtetR::*P_{tetA}*::mCherry* $P_{hmp::}$*gfp*. P_{dps}*::gfp-ssrA,* gfp^+, and $P_{hmp::}$*gfp* reporter constructs have
448 been previously described (16), and are all inserted into the pACYC184 plasmid.

449

450 *In vitro reporter characterization.* Once subcultures reached exponential phase (2h growth), the
451 indicated doses of doxycycline (Dox; 0.01 µg/mL, 0.1 µg/mL, or 1 µg/mL) or
452 anhydrotetracycline (ATc; 0.1 µg/mL, 1 µg/mL, or 2 µg/mL) were added to samples to promote
453 mCherry dilution, with one sample left untreated as a control. Samples were incubated at 37°C
454 with rotation throughout the time course, and time points of 0, 0.5, 1, 2, 3, and 4h post-antibiotic
455 treatment were taken. For each time point, 600 µL from each sample was pelleted and
456 resuspended in 600 µL of PBS. 200 µL of each sample was then pipetted into 3 wells of a black
457 walled, clear bottom 96 well plate, and analyzed using a Synergy Microplate Reader (Biotek
458 Instruments) for OD_{600} and fluorescence signal measurements. Optical density (A_{600nm}) was used
459 to approximate cell number, and mCherry fluorescence was detected with 560nm
460 excitation/610nm emission. All experiments were repeated in triplicate to generate a total of
461 three independent data sets, or nine replicates. In strains of Yptb also containing a GFP reporter,
462 GFP fluorescence was detected with 480nm excitation/520nm emission.
463
464 *Induction of hmp using nitric oxide donor compound.* Diluted subcultures were prepared as
465 described above, and after 1h subculture, were either treated with the nitric oxide donor
466 compound DETA-NONOate (2.5 mM dose), or were left untreated. After another hour of
467 incubation, each culture was evenly split into two separate tubes. Samples were then further
468 treated with either ATc (1 µg/mL dose) or left untreated, for a total of four different treatment
469 groups: +NO/+ATc, +NO/-ATc, -NO/+ATc, -NO/-ATc. OD and fluorescence of each sample
470 were measured every 2h as described above. Cells were also prepared for fluorescence
471 microscopy at every time point, as described below.
472

473 *Fluorescence microscopy: bacteria.* To visualize individual bacterial cells, 500 µL from each
474 sample was pelleted, resuspended in 4% paraformaldehyde (PFA), and incubated overnight at 4°
475 C for fixation. Agarose pads were prepared by placing two pieces of tape approximately 1 cm
476 apart on slides, pipetting 25 µL of 1% agarose in PBS, and placing a glass coverslip over the
477 area. After leaving the agarose to solidify for 20 min, the coverslips and tape were peeled off and
478 the agarose was trimmed to 1 cm^2 squares. PFA-fixed bacteria were pelleted, resuspended in 50
479 µL PBS, and 5 µL of sample was pipetted onto each agarose pad. Bacteria were imaged with the
480 63x oil immersion objective, using a Zeiss Axio Observer.Z1 (Zeiss) fluorescent microscope
481 with Colibri.2 LED light source and an ORCA-R^2 digital CCD camera (Hamamatsu). Five
482 images were taken of each sample in distinct fields of view, using DIC, GFP, and mCherry
483 channels. Volocity image analysis software was used to specifically select individual bacterial
484 cells and quantify the fluorescent signal associated with each cell.
485
486 *Murine model of systemic infection.* The following strains were used for mouse infections: *Y.*
487 *pseudotuberculosis tetR::*P_{tetA}*::mCherry-ssrA gfp*$^+$ (22)*, revtetR::*P_{tetA}*::mCherry gfp*$^+$*,* and
488 *revtetR::*P_{tetA}*::mCherry* $P_{hmp::}$*gfp*. Six to eight week old female C57BL/6 mice were obtained
489 from Jackson Laboratories (Bar Harbor, ME). All animal studies were approved by the
490 Institutional Animal Care and Use Committee of Johns Hopkins University. Mice were injected
491 intravenously with 10^3 bacteria for all experiments. After 48 hours, mice were treated with the
492 indicated dose (4mg/kg, equates to approximately 72µg in 100µl sterile PBS) of Dox or ATc. At
493 the indicated timepoints, either 4h or 24h post-treatment, mice were euthanized via both lethal
494 dose of isoflurane and cervical dislocation, and spleens were removed, halved, and processed for
495 histology, or homogenized to quantify CFUs.

496

497 *Histology.* Harvested spleen halves were fixed in 4% PFA overnight at 4° C, and were embedded
498 using Sub Xero OCT compound (Mercedes Medical), frozen on dry ice, and stored at -80°C.
499 Spleens were cross-sectioned into 10 um sections using a cryostat microtome; one representative
500 section was imaged per mouse. To visualize reporters, sections were thawed in PBS, stained with
501 Hoechst at a 1:10,000 dilution, washed in PBS, and coverslips were mounted using ProLong
502 Gold (Life Technologies). Images were taken of all microcolonies within each section with a 63x
503 oil immersion objective, using a Zeiss Axio Observer.Z1 (Zeiss) fluorescent microscope with
504 Colibri.2 LED light source, an Apotome.2 (Zeiss) for optical sectioning, and an ORCA-R^2 digital
505 CCD camera (Hamamatsu).

506

507 *Image analysis.* For *in vitro* experiments, Volocity image analysis software was used to identify
508 single bacterial cells in each image taken, and to determine the total fluorescence intensity level
509 in each bacterium for both mCherry and GFP. For *in vivo* experiments, Fiji image analysis
510 software was used to quantify the signal intensity of each channel at the centroid and periphery
511 of each microcolony, to generate relative signal intensities of fluorescent reporters. This was
512 done by selecting a small representative area (0.01pixels^2) at the centroid and periphery of each
513 microcolony. Centroid bacteria were defined as being surrounded only by other bacteria.
514 Peripheral bacteria were defined as being in contact with host cells (**Figure 5D**). All data was
515 analyzed and graphed, and all statistical analyses performed, using GraphPad Prism 9.

516

517 **Author Contributions.** Conceptualization: BL, RKD, KMD; Formal Analysis: BL, KMD;
518 Funding Acquisition and Supervision: KMD; Investigation: BL, RKD, KMD; Methodology: BL,

519 KMD; Writing – Original Draft Preparation: BL, KMD; Writing – Review & Editing: BL, RKD,
520 KMD.
521
522 **Acknowledgments.** We thank the members of the Davis lab, who provided feedback and
523 suggestions during the final steps of manuscript preparation. The authors of this manuscript
524 declare no conflicts of interest. This work was supported by a NIAID K22 Career Transition
525 Award (1K22AI123465-01).

526 **Figure Legends**

527 **Figure 1. The revTetR reporter can be used to visualize differential bacterial growth rates**
528 ***in vitro* with mCherry fluorescence dilution. (A)** The revTetR reporter was created by
529 introducing two mutations (E15A and L17G) in the wild-type tetR sequence, which results in
530 constitutive mCherry expression in the absence of tetracyclines (-Tet). Tetracycline addition
531 (+Tet) promotes revTetR binding and repression of mCherry transcription. **(B)** After tetracycline
532 addition (+Dox/ATc), fast-growing/dividing bacteria (top row, red circles) will partition
533 mCherry equally into daughter cells with each cell division event, resulting in dilution. Slow-
534 growing/non-dividing cells will retain a high level of mCherry (bottom row). Exponential phase
535 cultures of the revTetR *dps* strain were treated with the indicated ATc doses at 0h (hours, h),
536 aliquots were taken at the indicated timepoints to detect **(C)** optical density by absorbance
537 (A_{600nm}), **(D)** mCh fluorescence (normalized by dividing total fluorescence by OD values,
538 untreated value set to 100%), and **(E)** GFP fluorescence normalized to OD. **(C-E)**: Data shown
539 from 9 replicates. **(F)** Cells treated with the indicated doses of ATc for 4h were fixed for
540 fluorescence microscopy. Sum single cell mCherry signal is shown. **(G)** Sum single cell GFP
541 signal is shown. **(H)** Correlation plot depicting single cell sum mCherry and sum GFP signals.
542 **(F-H):** Data shown from three biological replicates. Mean and standard deviation are shown.
543 Statistics: **(C-E)** Two-way ANOVA with Tukey's multiple comparison test, comparisons made
544 between 2µg/ml and other groups; **(F-G)** Kruskal-Wallis one-way ANOVA with Dunn's post-
545 test; **(H)** linear regression with R^2 value and slope of best-fit line, significantly non-zero slope
546 indicates values are correlated. ****p<.0001, **p<.01, *p<.05, n.s.: not-significant.
547

548 **Figure 2. Growth inhibition with doxycycline promotes mCherry fluorescence**
549 **accumulation.** Exponential phase cultures of the revTetR *dps* strain were treated with the
550 indicated doses of doxycycline (Dox) at 0h (hours, h), aliquots were taken at the indicated
551 timepoints to detect **(A)** optical density by absorbance (A_{600nm}), **(B)** mCh fluorescence
552 (normalized by dividing total fluorescence by OD values, untreated value set to 100%), and **(C)**
553 GFP fluorescence normalized to OD. **(A-C)**: Data shown from 9 replicates. **(D)** Cells treated
554 with the indicated doses of Dox for 4h were fixed for fluorescence microscopy. Sum single cell
555 mCherry signal is shown. **(E)** Correlation plot depicting single cell sum mCherry and sum GFP
556 signals. **(D-E):** Data shown from three biological replicates. Mean and standard deviation are
557 shown. Statistics: **(A-C)** Two-way ANOVA, Tukey's multiple comparison test, comparisons
558 shown between untreated (0µg/ml) and 1µg/ml Dox; **(D)** Kruskal-Wallis one-way ANOVA with
559 Dunn's post-test; **(E)** linear regression with R^2 value and slope of best-fit line, significantly non-
560 zero slope indicates values are correlated. ****p<.0001, ***p<.001, **p<.01, *p<.05, n.s.: not-
561 significant.
562
563 **Figure 3. Gentamicin treatment confirms mCherry fluorescence levels are heightened in**
564 **growth arrested cells.** Overnight cultures of the revTetR *dps* strain were diluted 1:100 and
565 treated with the indicated doses of gentamicin at 0h (hours, h), aliquots were taken at the
566 indicated timepoints to detect **(A)** optical density by absorbance (A_{600nm}) and **(B)** mCherry (mCh)
567 fluorescence, normalized by dividing total fluorescence by OD values. Mean and standard
568 deviation are shown. **(C)** Exponential phase cultures of the revTetR *dps* strain were treated with
569 40µg/ml gentamicin (gent) 1h, and an aliquot of cells were fixed for fluorescence microscopy.
570 Sum single cell mCherry signal is shown. Median value/group is highlighted. **(D)** After 1h

571 gentamicin treatment, cultures of the revTetR *dps* strain were treated with 1µg/ml ATc at 0h, and
572 aliquots were taken at the indicated timepoints to detect optical density by absorbance (A_{600nm}).
573 Mean and standard deviation are shown. **(E)** Cells incubated +/-ATc for 4h were fixed for
574 fluorescence microscopy. Sum single cell mCherry signal is shown. Median value/group is
575 highlighted. Data shown from three biological replicates. Statistics: **(B)** Two-way ANOVA,
576 Tukey's multiple comparison test, comparisons shown between untreated (0µg/ml) and 40µg/ml
577 gent; **(C)** Mann-Whitney; **(E)** Kruskal-Wallis one-way ANOVA with Dunn's post-test;
578 ****p<.0001, ***p<.001, **p<.01, *p<.05.
579
580 **Figure 4. Nitric oxide-stressed cells divide at a slower rate than unstressed cells. (A)**
581 Schematic of experimental design. Overnight cultures of the revTetR P_{hmp}*::gfp* strain were
582 diluted 1:100 and grown for 1h prior to NO donor addition, then cultured one addition hour in
583 the presence (+NO) or absence (-NO) of NO. Cultures were then split, and either treated with
584 1µg/ml ATc (+ATc) or left untreated (-ATc). **(B)** Aliquots were taken at the indicated timepoints
585 to detect optical density by absorbance (A_{600nm}). Mean and standard deviation are shown. **(C)**
586 Aliquots of cells were fixed at the indicated timepoints after ATc addition for fluorescence
587 microscopy. Sum single cell mCherry signal is shown. Median value/group is highlighted. **(D)**
588 Correlation plots depicting single cell sum mCherry and mean GFP signals. Comparisons were
589 made for NO-treated cells (+NO) in the presence (+ATc) and absence (-ATc) of ATc, cells were
590 imaged at the indicated timepoints after ATc addition. Values were normalized to the max signal
591 intensity detected in samples, which is represented as a value of 1.0. All data shown represents
592 three biological replicates. Statistics: **(B)** Two-way ANOVA, Tukey's multiple comparison test,
593 comparisons shown between untreated (-NO) and NO donor treated (+NO) samples; **(C)**

594 Kruskal-Wallis one-way ANOVA with Dunn's post-test; **(D)** linear regression with R^2 value and
595 slope of best-fit line, significantly non-zero slope indicates values are correlated. ****p<.0001,
596 *p<.05, n.s.: not-significant.
597
598 **Figure 5. Low doses of doxycycline and anhydrotetracycline diffuse evenly across**
599 **microcolonies and do not inhibit bacterial growth.** C57BL/6 mice were infected intravenously
600 with the TetON *gfp*$^+$ strain and a single dose of Dox (4mg/kg) or ATc (4 mg/kg) was
601 administered intraperitoneally at 48h post-inoculation. Spleens were harvested at the indicated
602 timepoints after treatment. **(A)** Schematic of the TetON reporter: addition of tetracycline relieves
603 TetR repression and allows for *mCherry* transcription. **(B)** CFU/spleen quantification at the
604 indicated timepoints post-treatment. Dotted line: limit of detection, dots: individual mice. **(C)**
605 Reporter signal was detected with fluorescence microscopy and is shown as the ratio of TetON
606 (mCherry)/GFP signal at the centroid and periphery of microcolonies. Timepoints indicate time
607 post-treatment with ATc (left panel) or Dox (right panel). Dotted line: equivalent levels of
608 mCherry and GFP signal. Each dot: individual microcolony. Mean and standard deviation are
609 shown. **(D)** Representative images; cells outside the dotted line are defined as peripheral. Dataset
610 represents 4-5 mice/group, collected from two independent experiments; 2-8 microcolonies were
611 analyzed/spleen from a single cross-section of tissue. Statistics: **(B)** Kruskal-Wallis one-way
612 ANOVA with Dunn's post-test; **(C)** Wilcoxon matched-pairs; *p<.05, n.s.: not-significant.
613
614 **Figure 6. revTetR signal appears to increase in both the centroid and periphery of**
615 **microcolonies.** C57BL/6 mice were infected intravenously with the revTetR *gfp*$^+$ strain and a
616 single dose of ATc (4 mg/kg) was administered intraperitoneally at 48h post-inoculation. Spleens

617 were harvested at the indicated timepoints after treatment to quantify CFUs and prepare tissue
618 for fluorescence microscopy. **(A)** CFU/spleen quantification at the indicated timepoints post-
619 treatment. Dotted line: limit of detection, dots: individual mice, horizontal lines: median values.
620 **(B)** Reporter signal at 4h quantified using the ratio of revTetR (mCherry)/GFP signal at the
621 centroid and periphery of microcolonies. Dotted line: equivalent levels of mCherry and GFP
622 signal. Each dot: individual microcolony. Mean and standard deviation are shown. **(C)** Reporter
623 signal at 24h quantified using ratio of revTetR (mCherry)/GFP signal at the centroid and
624 periphery of microcolonies. Mean and standard deviation are shown. **(D)** Representative images.
625 Dataset represents 4-6 mice/group, collected from three independent experiments; 2-13
626 microcolonies were analyzed/spleen from a single cross-section of tissue. Statistics: **(A)** Kruskal-
627 Wallis one-way ANOVA with Dunn's post-test; **(B-C)** Wilcoxon matched-pairs; **p<.01,
628 *p<.05, n.s.: not-significant.
629
630 **Figure 7. NO stress correlates with heightened mCherry signal accumulation and slowed**
631 **cell division rates.** Mice were infected with the revTetR P_{hmp}*::gfp* strain and a single dose of
632 ATc (4 mg/kg) was administered intraperitoneally at 48h post-inoculation. Spleens were
633 harvested at the indicated timepoints after treatment and prepared for fluorescence microscopy.
634 **(A)** CFU/spleen quantification. Dotted line: limit of detection, dots: individual mice. **(B)**
635 Reporter signal at 4h quantified using ratio of periphery/centroid signal for either mCherry
636 (mCh) or GFP. Dotted line: equivalent levels of mCherry and GFP signal. Each dot: individual
637 microcolony. **(C)** Reporter signal at 24h quantified using ratio of periphery/centroid signal for
638 either mCh or GFP. **(D-G)** Correlation plots depicting single cell sum revTetR (mCherry) and
639 Hmp (GFP) signals at the indicated timepoints, comparing +/- ATc treatment. Graphs represent

640 either centroid or peripheral values, dots: individual microcolonies. **(H)** Representative images
641 with the green and red channels shown alongside merged images for 24h post-treatment images.
642 Dataset represents 5-6 mice/group, collected from three independent experiments; 3-8
643 microcolonies were analyzed/spleen from a single cross-section of tissue. Median values shown
644 with horizontal lines. Statistics: (A-C) Kruskal-Wallis one-way ANOVA with Dunn's post-test
645 **(D-G)** linear regression with R^2 value and slope of best-fit line, significantly non-zero slope
646 indicates values are correlated. **p<.01, n.s.: not-significant.
647
648 **Supplemental Figure 1. Hmp reporter signal is heightened in bacteria treated with the NO**
649 **donor compound.** Cultures of the revTetR P_{hmp}*::gfp* strain were cultured one hour in the
650 presence of NO (+NO treatment), then split, and either treated with 1µg/ml ATc (+ATc) or left
651 untreated (-ATc). Aliquots of cells were fixed at the indicated timepoints after ATc addition for
652 fluorescence microscopy. Single cell fold change in GFP signal with NO treatment is shown,
653 compared to untreated cells. Dotted line at a value of 1 is the mean GFP signal from individual
654 untreated cells. Median value/group is highlighted.
655
656 **References**
657
658 1. Balaban N, Merrin J, Chait R, Kowalik L, Leibler S. 2004. Bacterial persistence as a
659 phenotypic switch. Science 305:1622-5.

660 2. Goerke C, Wolz C. 2010. Adaptation of *Staphylococcus aureus* to the cystic fibrosis
661 lung. Int J Med Microbiol 300:520-5.

662 3. Harms A, Maisonneuve E, Gerdes K. 2016. Mechanisms of bacterial persistence during
663 stress and antibiotic exposure. Science 354(6318):aaf4268.

664 4. Lopatkin A, Stokes J, Zheng E, Yang J, Takahashi M, You L, Collins J. 2019. Bacterial
665 metabolic state more accurately predicts antibiotic lethality than growth rate. Nat
666 Microbiol 4:2109-2117.

667 5. Arnoldini M, Vizcarra I, Peña-Miller R, Stocker N, Diard M, Vogel V, Beardmore R,
668 Hardt W, Ackermann M. 2014. Bistable expression of virulence genes in *Salmonella*
669 leads to formation of an antibiotic-tolerant subpopulation. PLoS Biol 12:e1001928.

670 6. Nguyen D, Joshi-Datar A, Lepine F, Bauerle E, Olakanmi O, Beer K, McKay G, Siehnel
671 R, Schafhauser J, Wang Y, Britigan B, Singh P. 2011. Active starvation responses
672 mediate antibiotic tolerance in biofilms and nutrient-limited bacteria. Science 334:982-
673 986.

674 7. Sánchez-Romero M, Casadesús J. 2014. Contribution of phenotypic heterogeneity to
675 adaptive antibiotic resistance. Proc Natl Acad Sci 111:355-60.

676 8. Claudi B, Spröte P, Chirkova A, Personnic N, Zankl J, Schürmann N, Schmidt A,
677 Bumann D. 2014. Phenotypic variation of *Salmonella* in host tissues delays eradication
678 by antimicrobial chemotherapy. Cell 158:722-33.

679 9. Kaiser P, Regoes R, Dolowschiak T, Wotzka S, Lengefeld J, Slack E, Grant A,
680 Ackermann M, Hardt W. 2014. Cecum lymph node dendritic cells harbor slow-growing
681 bacteria phenotypically tolerant to antibiotic treatment. PLoS Biol 12:e1003532.

682 10. Manina G, Dhar N, McKinney J. 2015. Stress and host immunity amplify *Mycobacterium*
683 *tuberculosis* phenotypic heterogeneity and induce nongrowing metabolically active
684 forms. Cell Host Microbe 17:32-46.

685 11. Perry W, Spraggins J, Sheldon J, Grunenwald C, Heinrichs D, Cassat J, Skaar E, Caprioli
686 R. 2019. *Staphylococcus aureus* exhibits heterogeneous siderophore production within
687 the vertebrate host. Proc Natl Acad Sci 116:21980-21982.

688 12. Cunrath O, Bumann D. 2019. Host resistance factor SLC11A1 restricts *Salmonella*
689 growth through magnesium deprivation. Science 366:995-999.

690 13. Rosenthal A, Qi Y, Hormoz S, Park J, Li S, Elowitz M. 2018. Metabolic interactions
691 between dynamic bacterial subpopulations. Elife 7:e33099.

692 14. Stewart P, White B, Boegli L, Hamerly T, Williamson K, Franklin M, Bothner B, James
693 G, Fisher S, Vital-Lopez F, Wallqvist A. 2019. Conceptual model of biofilm antibiotic
694 tolerance that integrates phenomena of diffusion, metabolism, gene expression, and
695 physiology. J Bacteriol 201:e00307-19.

696 15. Burton N, Schürmann N, Casse O, Steeb A, Claudi B, Zankl J, Schmidt A, Bumann D.
697 2014. Disparate impact of oxidative host defenses determines the fate of *Salmonella*
698 during systemic infection of mice. Cell Host Microbe 15:72-83.

699 16. Patel P, O'Hara B, Aunins E, Davis K. 2021. Modifying TIMER to generate a slow-
700 folding DsRed derivative for optimal use in quickly-dividing bacteria. PLoS Pathog
701 17:e1009284.

702 17. Davis K, Mohammadi S, Isberg R. 2015. Community behavior and spatial regulation
703 within a bacterial microcolony in deep tissue sites serves to protect against host attack.
704 Cell Host Microbe 17:21-31.

705 18. Rowe S, Wagner N, Li L, Beam J, Wilkinson A, Radlinski L, Zhang Q, Miao E, Conlon
706 B. 2020. Reactive oxygen species induce antibiotic tolerance during systemic
707 *Staphylococcus aureus* infection. Nat Microbiol 5(2):282-290.

708 19. Brauner A, Fridman O, Gefen O, Balaban N. 2016. Distinguishing between resistance,
709 tolerance and persistence to antibiotic treatment. Nat Rev Microbiol 14:320-30.

710 20. Fisher R, Gollan B, Helaine S. 2017. Persistent bacterial infections and persister cells.
711 Nat Rev Microbiol 15:453-64.

712 21. Stapels D, Hill P, Westermann A, Fisher R, Thurston T, Saliba A, Blommestein I, Vogel
713 J, Helaine S. 2018. *Salmonella* persisters undermine host immune defenses during
714 antibiotic treatment. Science 362:1156-1160.

715 22. Raneses J, Ellison A, Liu B, Davis K. 2020. Subpopulations of stressed *Y.*
716 *pseudotuberculosis* preferentially survive doxycycline treatment within host tissues.
717 mBio 11:e00901-20.

718 23. Henry T, Brynildsen M. 2016. Development of persister-FACSeq: a method to massively
719 parallelize quantification of persister physiology and its heterogeneity. Sci Rep 6:25100.

720 24. Luk C, Valenzuela C, Gil M, Swistak L, Bomme P, Chang Y, Mallet A, Enninga J. 2021.
721 *Salmonella* enters a dormant state within human epithelial cells for persistent infection.
722 PLoS Pathog 17(4):e1009550.

723 25. Schulte M, Olschewski K, Hensel M. 2021. Fluorescent protein-based reporters reveal
724 stress response of intracellular *Salmonella enterica* at level of single bacterial cells. Cell
725 Microbiol 23(3):e13293.

726 26. Zalis E, Nuxoll A, Manuse S, Clair G, Radlinski L, Conlon B, Adkins J, Lewis K. 2019.
727 Stochastic variation in expression of the tricarboxylic acid cycle produces persister cells.
728 MBio 10:e01930-19.

729 27. Helaine S, Thompson J, Watson K, Liu M, Boyle C, Holden D. 2010. Dynamics of
730 intracellular bacterial replication at the single cell level. Proc Natl Acad Sci 107:3746-51.

731 28. Roostalu J, Jöers A, Luidalepp H, Kaldalu N, Tenson T. 2008. Cell division in
732 *Escherichia coli* cultures monitored at single cell resolution. BMC Microbiol 8:68.

733 29. Helaine S, Holden D. 2013. Heterogeneity of intracellular replication of bacterial
734 pathogens. Curr Opin Microbiol 16:184-91.

735 30. Saliba A, Li L, Westermann A, Appenzeller S, Stapels D, Schulte L, Helaine S, Vogel J.
736 2016. Single-cell RNA-seq ties macrophage polarization to growth rate of intracellular
737 *Salmonella*. Nat Microbiol 2:16206.

738 31. Gonzalez R, Lane M, Wagner N, Weening E, Miller V. 2015. Dissemination of a highly
739 virulent pathogen: tracking the early events that define infection. PLoS Pathog
740 11:e1004587.

741 32. McVicker G, Prajsnar T, Williams A, Wagner N, Boots M, Renshaw S, Foster S. 2014.
742 Clonal expansion during *Staphylococcus aureus* infection dynamics reveals the effect of
743 antibiotic intervention. PLoS Pathog 10:e1003959.

744 33. Pollitt E, Szkuta P, Burns N, Foster S. 2018. *Staphylococcus aureus* infection dynamics.
745 PLoS Pathog 14(6):e1007112.

746 34. Capron J, Delamarre J, Delcenserie R, Gineston J, Dupas J, Lorriaux A. 1981. Liver
747 absess complicating *Yersinia pseudotuberculosis* ileitis. Gastroenterology 81:150-152.

748 35. Hubbert W, Petenyi C, Glasgow L, Uyeda C, Creighton S. 1971. *Yersinia*
749 *pseudotuberculosis* infection in the United States. Septicemia, appendicitis, and
750 mesenteric lymphadenitis. Am J Trop Med Hyg 20:679-684.

751 36. Paff J, Triplett D, Saari T. 1976. Clinical and laboratory aspects of *Yersinia*
752 *pseudotuberculosis* infections, with a report of two cases. Am J Clin Pathol 66:101-110.

753 37. Barnes P, Bergman M, Mecsas J, Isberg R. 2006. *Yersinia pseudotuberculosis*
754 disseminates directly from a replicating bacterial pool in the intestine. J Exp Med
755 203:1591-1601.

756 38. Peterson L, Philip N, DeLaney A, Wynosky-Dolfi M, Asklof K, Gray F, Choa R, Bjanes
757 E, Buza E, Hu B, Dillon C, Green D, Berger S, Gough P, Bertin J, Brodsky I. 2017.
758 RIPK1-dependent apoptosis bypasses pathogen blockage of innate signaling to promote
759 immune defense. J Exp Med 214:3171-3182.

760 39. Zhang Y, Khairallah C, Sheridan B, van der Velden A, Bliska J. 2018. CCR2+
761 inflammatory monocytes are recruited to *Yersinia pseudotuberculosis* pyogranulomas and
762 dictate adaptive responses at the expense of innate immunity during oral infection. Infect
763 Immun 86:e00782-17.

764 40. Green E, Clark S, Crimmins G, Mack M, Kumamoto C, Mecsas J. 2016. Fis is essential
765 for *Yersinia pseudotuberculosis* virulence and protects against reactive oxygen species
766 produced by phagocytic cells during infection. PLoS Pathog 12:e1005898.

767 41. Resch M, Striegl H, Henssler E, Sevvana M, Egerer-Sieber C, Schiltz E, Hillen W,
768 Muller Y. 2008. A protein functional leap: how a single mutation reverses the function of
769 the transcription regulator TetR. Nucleic Acids Res 36:4390-401.

770 42. Scholz O, Henssler E, Bail J, Schubert P, Bogdanska-Urbaniak J, Sopp S, Reich M,
771 Wisshak S, Köstner M, Bertram R, Hillen W. 2004. Activity reversal of Tet repressor
772 caused by single amino acid exchanges. Mol Microbiol 53:777-789.

773 43. Almiron M, Link A, Furlong D, Kolter R. 1992. A novel DNA-binding protein with
774 regulatory and protective roles in starved *Escherichia coli*. Genes Dev 6:2646-54.

775 44. Nair S, Finkel S. 2004. Dps protects cells against multiple stresses during stationary
776 phase. J Bacteriol 186:4192-8.

777 45. Karas V, Westerlaken I, Meyer A. 2015. The DNA-Binding Protein from Starved Cells
778 (Dps) Utilizes Dual Functions To Defend Cells against Multiple Stresses. J Bacteriol
779 197:3206-15.

780 46. Degenkolb J, Takahashi M, Ellestad G, Hillen W. 1991. Structural requirements of
781 tetracycline-Tet repressor interaction: determination of equilibrium binding constants for
782 tetracycline analogs with the Tet repressor. Antimicrob Agents Chemother 35:1591-5.

783 47. Rasmussen B, Noller H, Daubresse G, Oliva B, Misulovin Z, Rothstein D, Ellestad G,
784 Gluzman Y, Tally F, Chopra I. 1991. Molecular basis of tetracycline action: identification
785 of analogs whose primary target is not the bacterial ribosome. Antimicrob Agents
786 Chemother 35:2306-11.

787 48. Jones-Carson J, Yahashiri A, Kim J, Liu L, Fitzsimmons L, Weiss D, Vázquez-Torres A.
788 2020. Nitric oxide disrupts bacterial cytokinesis by poisoning purine metabolism. Sci
789 Adv 6:eaaz0260.

790 49. Davis K, Krupp J, Clark S, Isberg R. 2019. Iron-sulfur cluster repair contributes
791 to*Yersinia pseudotuberculosis* survival within deep tissues. Infect Immun 87(10)e00533-
792 19.

793 50. Rang C, Galen J, Kaper J, Chao L. 2003. Fitness cost of the green fluorescent protein in
794 gastrointestinal bacteria. Can J Microbiol 49:531-7.

795 51. Hecht A, Glasgow J, Jaschke P, Bawazer L, Munson M, Cochran J, Endy D, Salit M.
796 2017. Measurements of translation initiation from all 64 codons in *E. coli*. Nucleic Acids
797 Res 45:3615-3626.

798 52. Bolintineanu D, Volzing K, Vivcharuk V, Sayyed-Ahmad A, Srivastava P, Kaznessis Y.
799 2014. Investigation of Changes in Tetracycline Repressor Binding upon Mutations in the
800 Tetracycline Operator. J Chem Eng Data 59:3167-3176.

801 53. Sizemore C, Wissmann A, Gülland U, Hillen W. 1990. Quantitative analysis of Tn10 Tet
802 repressor binding to a complete set of *tet* operator mutants. Nucleic Acids Res 18:2875-
803 80.

804 54. Davidson R, Davis K. 2020. *Yersinia pseudotuberculosis*: Cultivation, Storage, and
805 Methods for Introducing DNA. Curr Protoc Microbiol 59(1):e122.
806

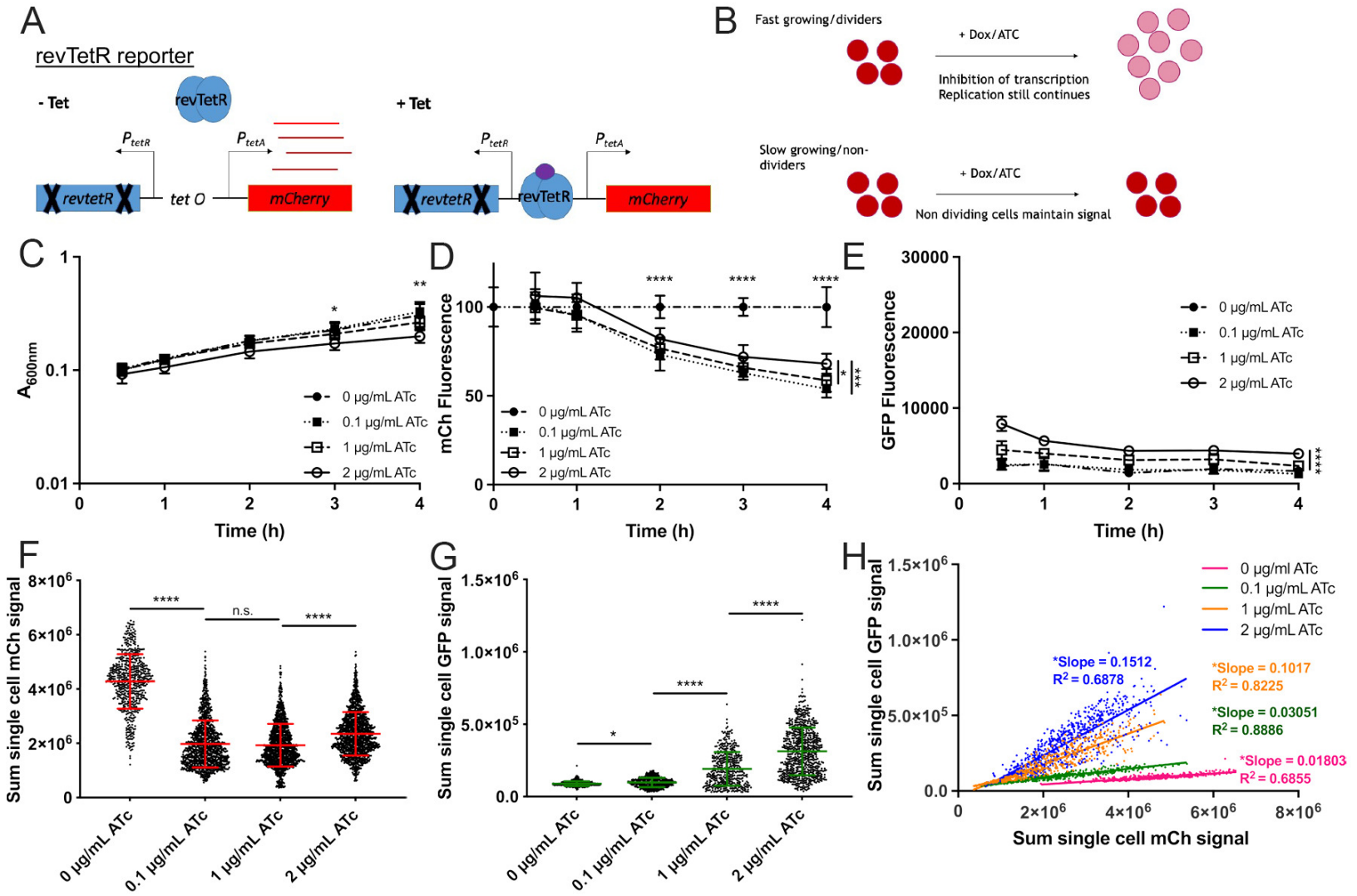

Figure 1. The revTetR reporter can be used to visualize differential bacterial growth rates *in vitro* with mCherry fluorescence dilution. (A) The revTetR reporter was created by introducing two mutations (E15A and L17G) in the wild-type tetR sequence, which results in constitutive mCherry expression in the absence of tetracyclines (-Tet). Tetracycline addition (+Tet) promotes revTetR binding and repression of mCherry transcription. **(B)** After tetracycline addition (+Dox/ATc), fast-growing/dividing bacteria (top row, red circles) will partition mCherry equally into daughter cells with each cell division event, resulting in dilution. Slow-growing/non-dividing cells will retain a high level of mCherry (bottom row). Exponential phase cultures of the revTetR *dps* strain were treated with the indicated ATc doses at 0h (hours, h), aliquots were taken at the indicated timepoints to detect **(C)** optical density by absorbance (A_{600nm}), **(D)** mCh fluorescence (normalized by dividing total fluorescence by OD values, untreated value set to 100%), and **(E)** GFP fluorescence normalized to OD. **(C-E)**: Data shown from 9 replicates. **(F)** Cells treated with the indicated doses of ATc for 4h were fixed for fluorescence microscopy. Sum single cell mCherry signal is shown. **(G)** Sum single cell GFP signal is shown. **(H)** Correlation plot depicting single cell sum mCherry and sum GFP signals. **(F-H):** Data shown from three biological replicates. Mean and standard deviation are shown. Statistics: **(C-E)** Two-way ANOVA with Tukey's multiple comparison test, comparisons made between 2µg/ml and other groups; **(F-G)** Kruskal-Wallis one-way ANOVA with Dunn's post-test; **(H)** linear regression with R^2 value and slope of best-fit line, significantly non-zero slope indicates values are correlated. ****p<.0001, **p<.01, *p<.05, n.s.: not-significant.

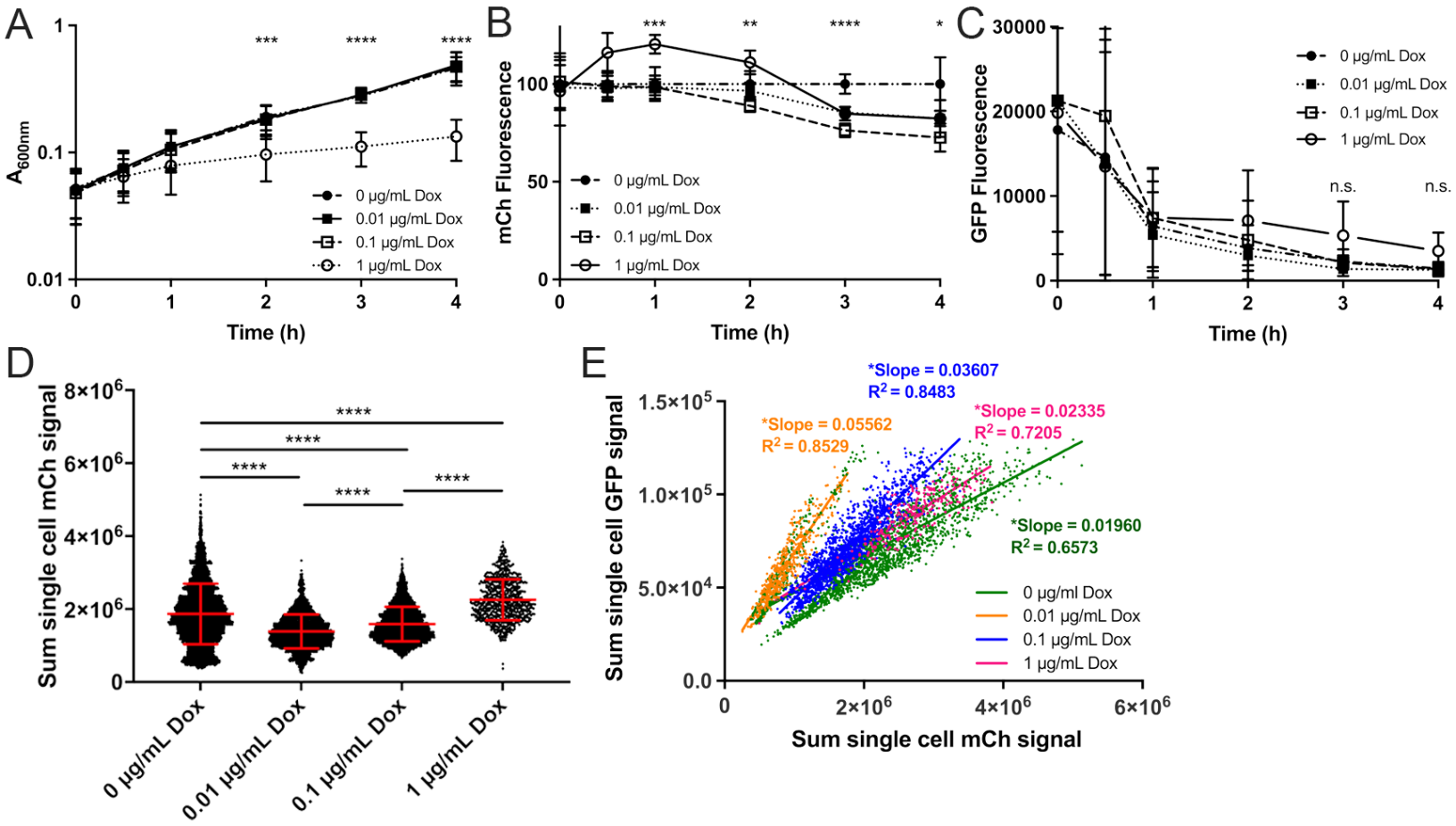

Figure 2. Growth inhibition with doxycycline promotes mCherry fluorescence accumulation. Exponential phase cultures of the revTetR *dps* strain were treated with the indicated doses of doxycycline (Dox) at 0h (hours, h), aliquots were taken at the indicated timepoints to detect **(A)** optical density by absorbance (A_{600nm}), **(B)** mCh fluorescence (normalized by dividing total fluorescence by OD values, untreated value set to 100%), and **(C)** GFP fluorescence normalized to OD. **(A-C)**: Data shown from 9 replicates. **(D)** Cells treated with the indicated doses of Dox for 4h were fixed for fluorescence microscopy. Sum single cell mCherry signal is shown. **(E)** Correlation plot depicting single cell sum mCherry and sum GFP signals. **(D-E):** Data shown from three biological replicates. Mean and standard deviation are shown. Statistics: **(A-C)** Two-way ANOVA, Tukey's multiple comparison test, comparisons shown between untreated (0µg/ml) and 1µg/ml Dox; **(D)** Kruskal-Wallis one-way ANOVA with Dunn's post-test; **(E)** linear regression with R^2 value and slope of best-fit line, significantly non-zero slope indicates values are correlated. ****p<.0001, ***p<.001, **p<.01, *p<.05, n.s.: not-significant.

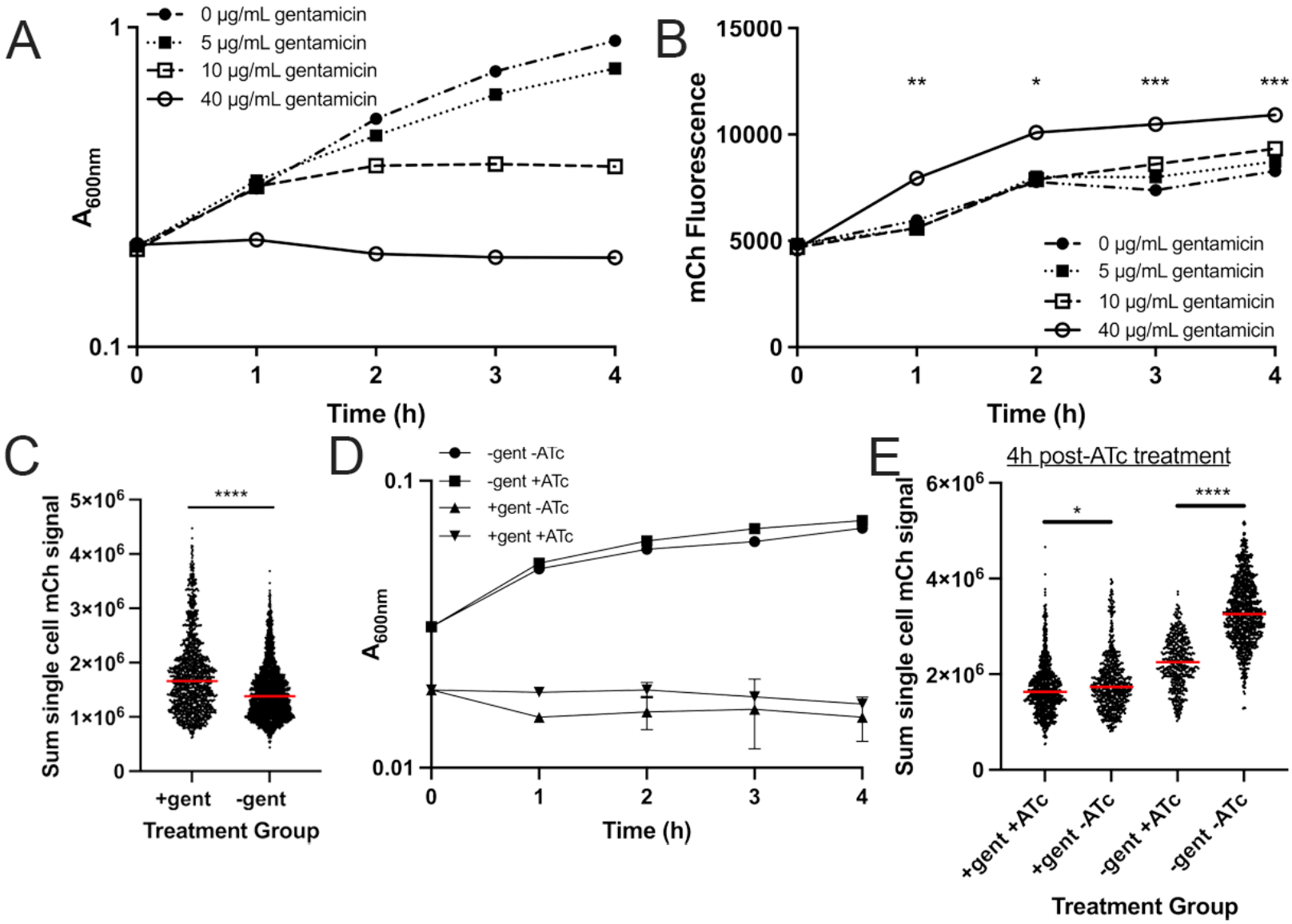

Figure 3. Gentamicin treatment confirms mCherry fluorescence levels are heightened in growth arrested cells. Overnight cultures of the revTetR *dps* strain were diluted 1:100 and treated with the indicated doses of gentamicin at 0h (hours, h), aliquots were taken at the indicated timepoints to detect **(A)** optical density by absorbance (A_{600nm}) and **(B)** mCherry (mCh) fluorescence, normalized by dividing total fluorescence by OD values. Mean and standard deviation are shown. **(C)** Exponential phase cultures of the revTetR *dps* strain were treated with 40µg/ml gentamicin (gent) 1h, and an aliquot of cells were fixed for fluorescence microscopy. Sum single cell mCherry signal is shown. Median value/group is highlighted. **(D)** After 1h gentamicin treatment, cultures of the revTetR *dps* strain were treated with 1µg/ml ATc at 0h, and aliquots were taken at the indicated timepoints to detect optical density by absorbance (A_{600nm}). Mean and standard deviation are shown. **(E)** Cells incubated +/-ATc for 4h were fixed for fluorescence microscopy. Sum single cell mCherry signal is shown. Median value/group is highlighted. Data shown from three biological replicates. Statistics: **(B)** Two-way ANOVA, Tukey's multiple comparison test, comparisons shown between untreated (0µg/ml) and 40µg/ml gent; **(C)** Mann-Whitney; **(E)** Kruskal-Wallis one-way ANOVA with Dunn's post-test; ****p<.0001, ***p<.001, **p<.01, *p<.05.

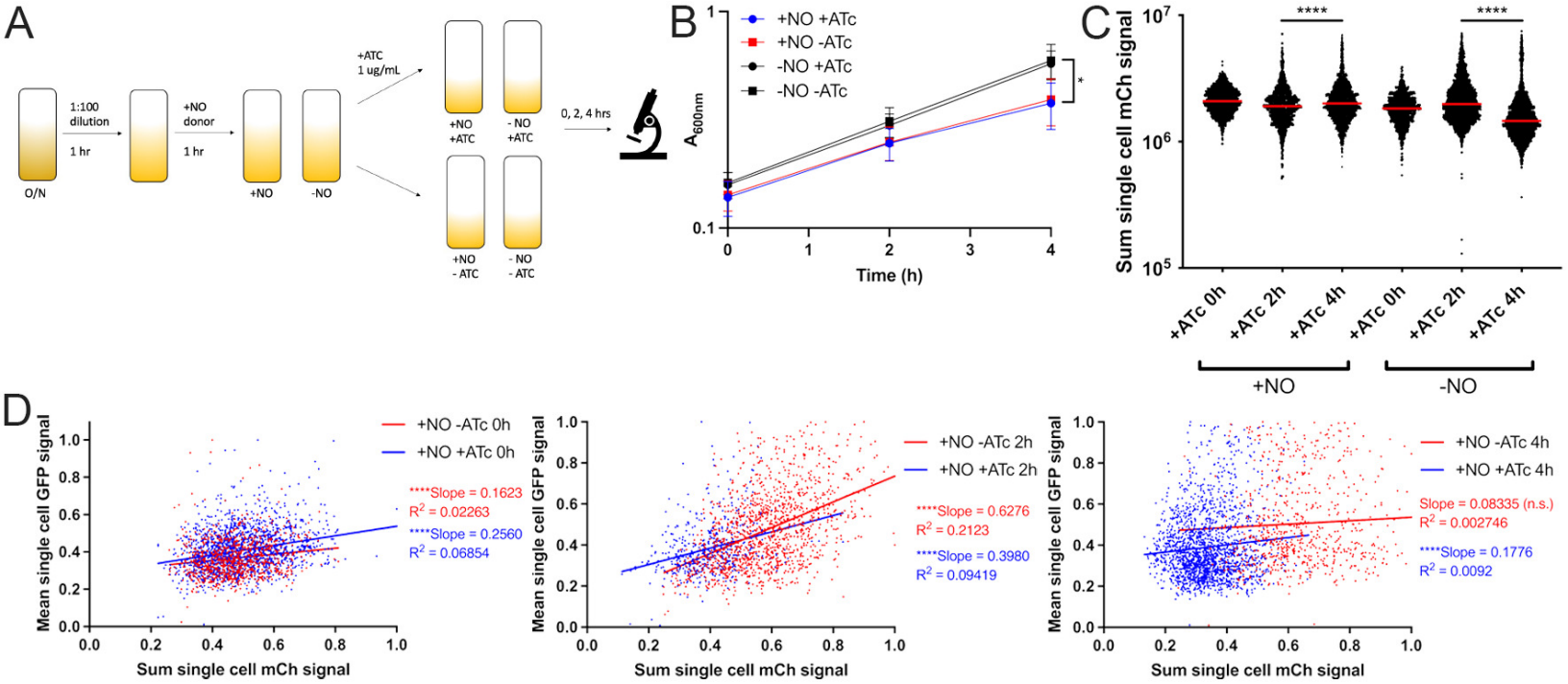

Figure 4. Nitric oxide-stressed cells divide at a slower rate than unstressed cells. (A) Schematic of experimental design. Overnight cultures of the revTetR P_{hmp}*::gfp* strain were diluted 1:100 and grown for 1h prior to NO donor addition, then cultured one addition hour in the presence (+NO) or absence (-NO) of NO. Cultures were then split, and either treated with 1µg/ml ATc (+ATc) or left untreated (-ATc). **(B)** Aliquots were taken at the indicated timepoints to detect optical density by absorbance (A_{600nm}). Mean and standard deviation are shown. **(C)** Aliquots of cells were fixed at the indicated timepoints after ATc addition for fluorescence microscopy. Sum single cell mCherry signal is shown. Median value/group is highlighted. **(D)** Correlation plots depicting single cell sum mCherry and mean GFP signals. Comparisons were made for NO-treated cells (+NO) in the presence (+ATc) and absence (-ATc) of ATc, cells were imaged at the indicated timepoints after ATc addition. Values were normalized to the max signal intensity detected in samples, which is represented as a value of 1.0. All data shown represents three biological replicates. Statistics: **(B)** Two-way ANOVA, Tukey's multiple comparison test, comparisons shown between untreated (-NO) and NO donor treated (+NO) samples; **(C)** Kruskal-Wallis one-way ANOVA with Dunn's post-test; **(D)** linear regression with R^2 value and slope of best-fit line, significantly non-zero slope indicates values are correlated. ****p<.0001, *p<.05, n.s.: not-significant.

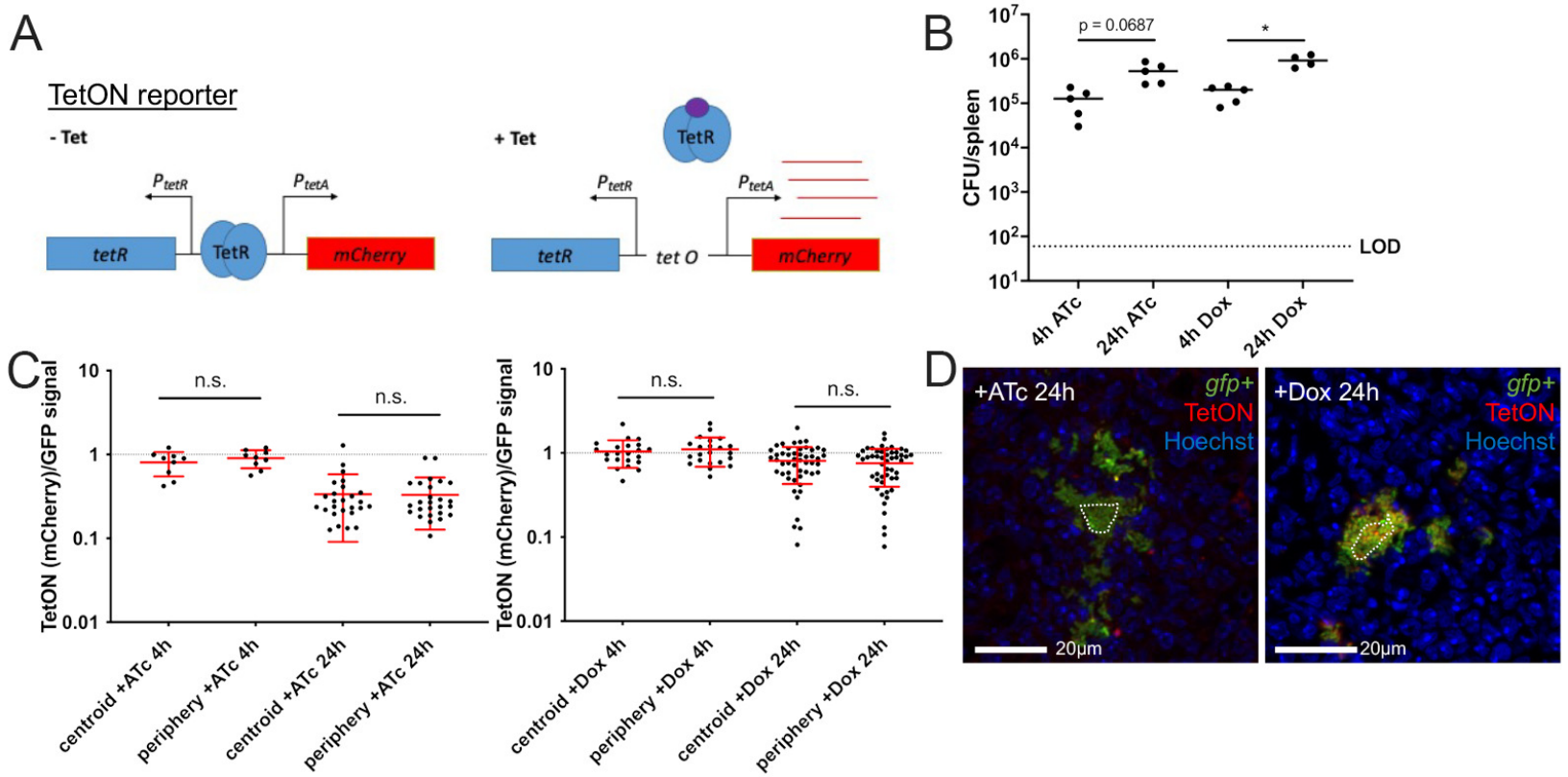

Figure 5. Low doses of doxycycline and anhydrotetracycline diffuse evenly across microcolonies and do not inhibit bacterial growth. C57BL/6 mice were infected intravenously with the TetON *gfp*⁺ strain and a single dose of Dox (4mg/kg) or ATc (4 mg/kg) was administered intraperitoneally at 48h post-inoculation. Spleens were harvested at the indicated timepoints after treatment. **(A)** Schematic of the TetON reporter: addition of tetracycline relieves TetR repression and allows for *mCherry* transcription. **(B)** CFU/spleen quantification at the indicated timepoints post-treatment. Dotted line: limit of detection, dots: individual mice. **(C)** Reporter signal was detected with fluorescence microscopy and is shown as the ratio of TetON (mCherry)/GFP signal at the centroid and periphery of microcolonies. Timepoints indicate time post-treatment with ATc (left panel) or Dox (right panel). Dotted line: equivalent levels of mCherry and GFP signal. Each dot: individual microcolony. Mean and standard deviation are shown. **(D)** Representative images; cells outside the dotted line are defined as peripheral. Dataset represents 4-5 mice/group, collected from two independent experiments; 2-8 microcolonies were analyzed/spleen from a single cross-section of tissue. Statistics: **(B)** Kruskal-Wallis one-way ANOVA with Dunn's post-test; **(C)** Wilcoxon matched-pairs; *p<.05, n.s.: not-significant.

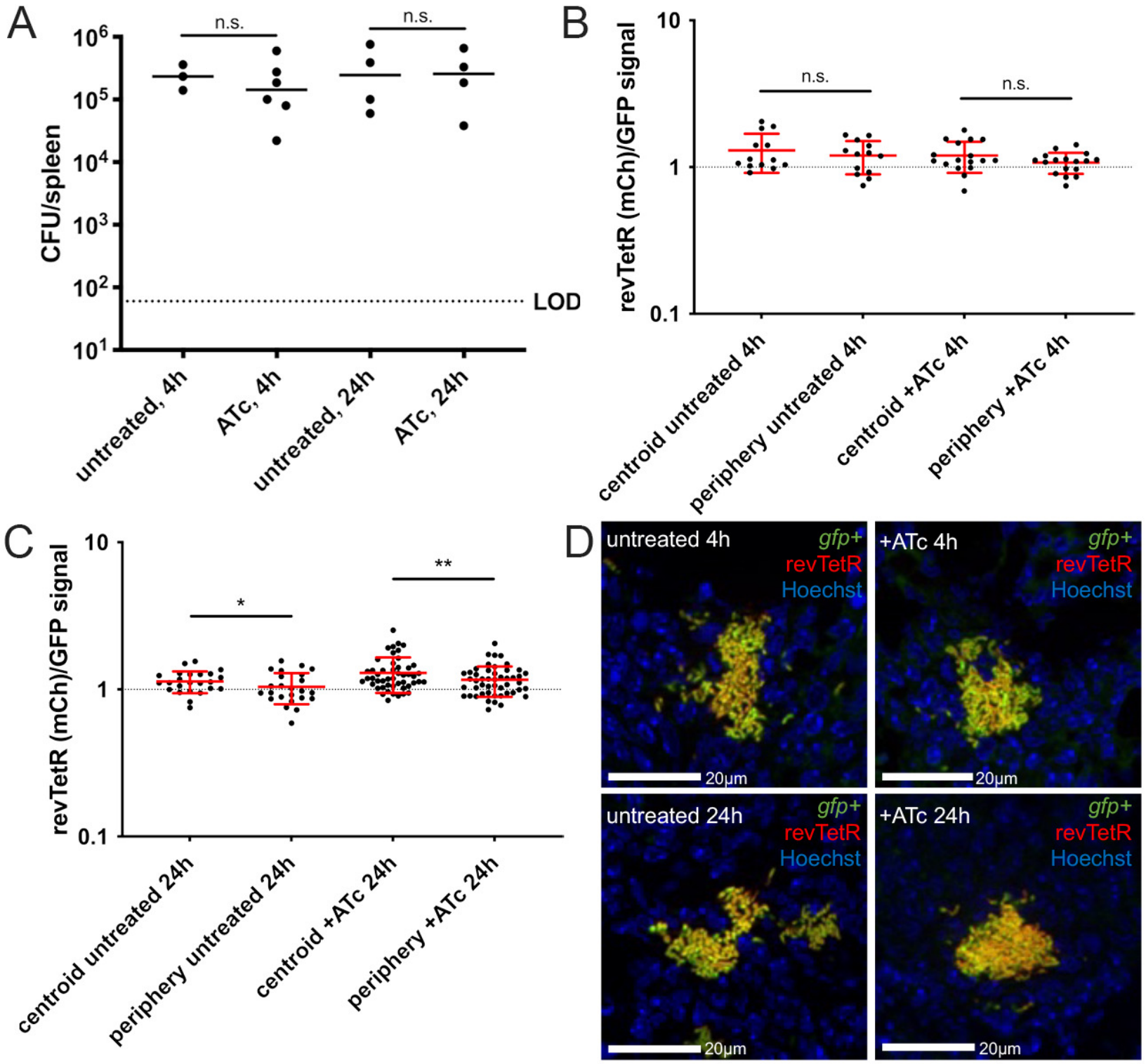

Figure 6. revTetR signal appears to increase in both the centroid and periphery of microcolonies. C57BL/6 mice were infected intravenously with the revTetR *gfp*⁺ strain and a single dose of ATc (4 mg/kg) was administered intraperitoneally at 48h post-inoculation. Spleens were harvested at the indicated timepoints after treatment to quantify CFUs and prepare tissue for fluorescence microscopy. **(A)** CFU/spleen quantification at the indicated timepoints post-treatment. Dotted line: limit of detection, dots: individual mice, horizontal lines: median values. **(B)** Reporter signal at 4h quantified using the ratio of revTetR (mCherry)/GFP signal at the centroid and periphery of microcolonies. Dotted line: equivalent levels of mCherry and GFP signal. Each dot: individual microcolony. Mean and standard deviation are shown. **(C)** Reporter signal at 24h quantified using ratio of revTetR (mCherry)/GFP signal at the centroid and periphery of microcolonies. Mean and standard deviation are shown. **(D)** Representative images. Dataset represents 4-6 mice/group, collected from three independent experiments; 2-13 microcolonies were analyzed/spleen from a single cross-section of tissue. Statistics: **(A)** Kruskal-Wallis one-way ANOVA with Dunn's post-test; **(B-C)** Wilcoxon matched-pairs; **p<.01, *p<.05, n.s.: not-significant.

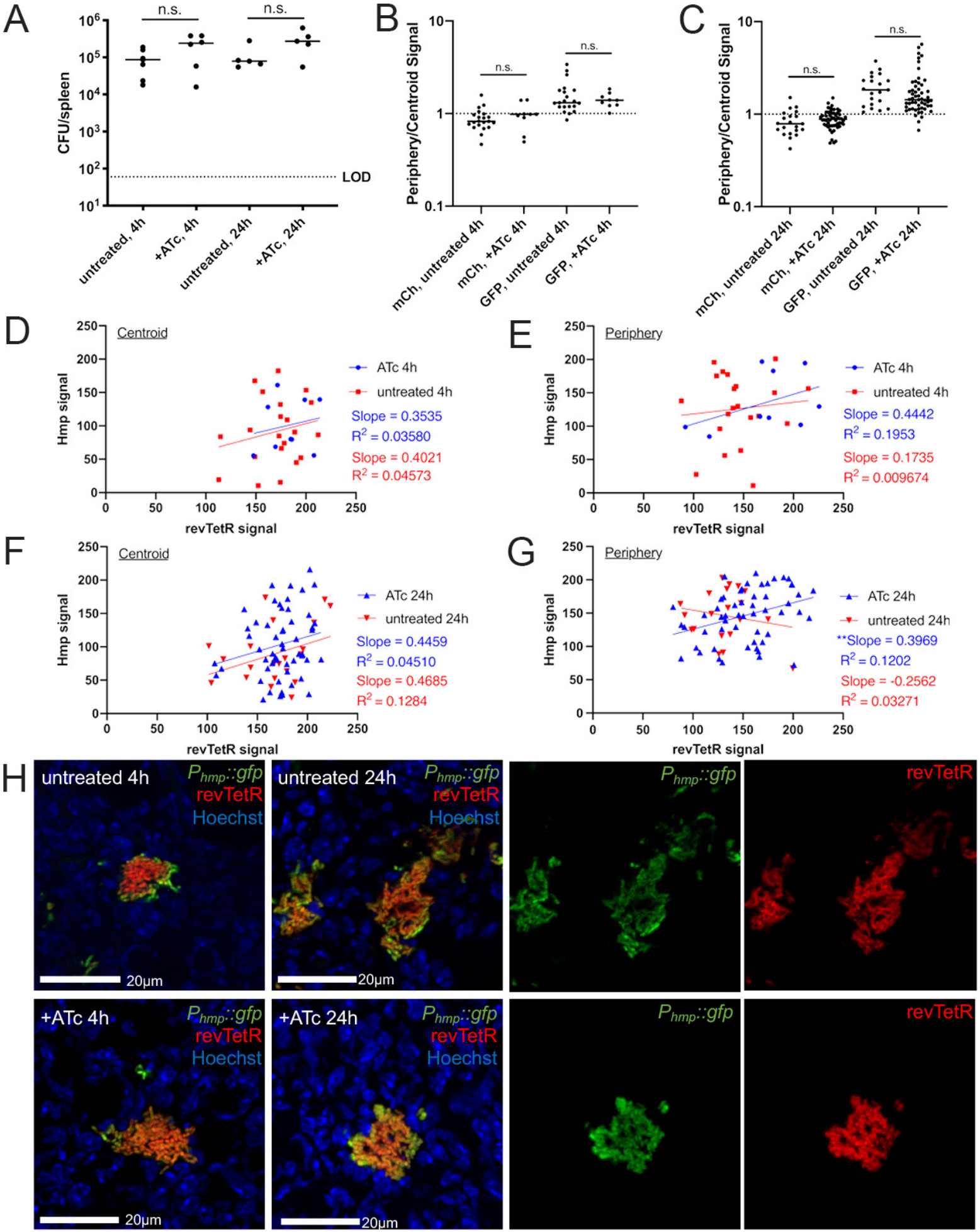

Figure 7. NO stress correlates with heightened mCherry signal accumulation and slowed cell division rates. Mice were infected with the revTetR P_{hmp}::*gfp* strain and a single dose of ATc (4 mg/kg) was administered intraperitoneally at 48h post-inoculation. Spleens were harvested at the indicated timepoints after treatment and prepared for fluorescence microscopy. **(A)** CFU/spleen quantification. Dotted line: limit of detection, dots: individual mice. **(B)** Reporter signal at 4h quantified using ratio of periphery/centroid signal for either mCherry (mCh) or GFP. Dotted line: equivalent levels of mCherry and GFP signal. Each dot: individual microcolony. **(C)** Reporter signal at 24h quantified using ratio of periphery/centroid signal for either mCh or GFP. **(D-G)** Correlation plots depicting single cell sum revTetR (mCherry) and Hmp (GFP) signals at the indicated timepoints, comparing +/- ATc treatment. Graphs represent either centroid or peripheral values, dots: individual microcolonies. **(H)** Representative images with the green and red channels shown alongside merged images for 24h post-treatment images. Dataset represents 5-6 mice/group, collected from three independent experiments; 3-8 microcolonies were analyzed/spleen from a single cross-section of tissue. Median values shown with horizontal lines. Statistics: (A-C) Kruskal-Wallis one-way ANOVA with Dunn's post-test **(D-G)** linear regression with R^2 value and slope of best-fit line, significantly non-zero slope indicates values are correlated. **p<.01, n.s.: not-significant.

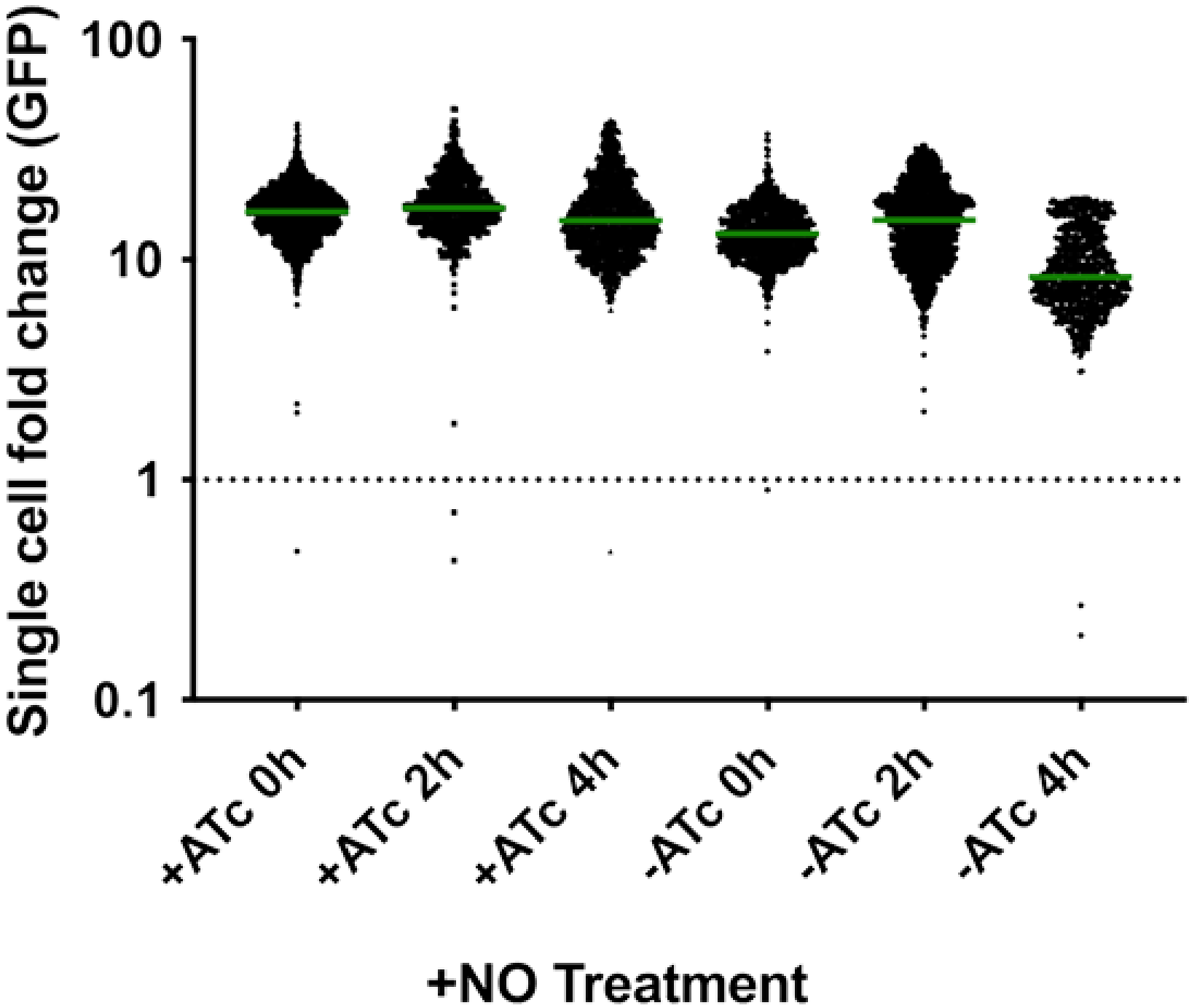

Supplemental Figure 1. Hmp reporter signal is heightened in bacteria treated with the NO donor compound. Cultures of the revTetR P_{hmp}*::gfp* strain were cultured one hour in the presence of NO (+NO treatment), then split, and either treated with 1µg/ml ATc (+ATc) or left untreated (-ATc). Aliquots of cells were fixed at the indicated timepoints after ATc addition for fluorescence microscopy. Single cell fold change in GFP signal with NO treatment is shown, compared to untreated cells. Dotted line at a value of 1 is the mean GFP signal from individual untreated cells. Median value/group is highlighted.